Resonance Raman Studies of Bis(pyridine) Adducts of Iron(II), Ruthenium(II), and Osmium(II) Octaethylporphyrins. Effects of Heavy-Metal Substitution on Porphyrin and Axial-Ligand Vibrational and Electronic Properties

G. Alan Schick[1a] and David F. Bocian*[1b]

Contribution from the Department of Chemistry, University of California, Riverside, California 92521. *Received August 24, 1983*

Abstract: Resonance Raman (RR) spectra are reported for the bis(pyridine) adducts of metallooctaethylporphyrins [(OEP)M(py)$_2$], where M = Fe(II), Ru(II), and Os(II), with excitation at a large number of wavelengths throughout the Soret and visible regions of the absorption spectra. Frequency variations in the porphyrin modes with metal substitution are interpreted in terms of changes in metal–porphyrin bonding (both σ and π), porphyrin core size, and metal charge. The Q-state RR excitation spectra (RRES) of many porphyrin fundamentals exhibit systematic variations in their relative intensities at Q(0,0) and Q(0,1) as the metal is changed. Simulations of the RRES indicate that the different amount of configuration interaction (CI) between the Q and B states for the three complexes (Fe > Ru > Os) is primarily responsible for the trends in the RRES (changes in the magnitude of the vibronic coupling for given modes also occur as the metal is varied but are of much less importance than changes in the CI). Bands attributed to resonance-enhanced pyridine (py) vibrations are observed in the RR spectra of all three complexes and exhibit systematic frequency trends with metal substitution. Normal coordinate calculations indicate that these trends are primarily due to kinematic effects, although potential energy effects due to changes in M→py σ bonding also contribute. RRES of the py modes covering the 405–630-nm region indicate the presence of M → py charge-transfer (CT) transitions at 514, 472, and 503 nm for the Fe(II), Ru(II), and Os(II) complexes, respectively, and near 600 nm for the Os(II) complex. The two CT transitions observed for the Os(II) complex are attributed to large spin–orbit coupling effects which split the $(t_{2g})^5$ excited-state configuration of the metal ion. Simulations of the RRES for the py modes are used to extract excited-state origin shifts, which are used in conjunction with normal coordinate calculations to determine excited-state geometry displacements for the py–M–py system. Pyridine ring bond displacements are calculated to be on the order of 0.010–0.020 Å and are essentially independent of metal.

I. Introduction

The physical and chemical properties of metalloporphyrin complexes have been the subject of considerable scientific interest during the past several decades.[2] Within the past few years effort has been directed toward characterizing the physicochemical properties of porphyrin complexes containing second- and third-row transition metals, particularly those with group 8 ions.[3-8] These latter complexes form very stable species with unusual axial ligation characteristics, including single-atom coordination (such as nitrido and oxo ligands)[5,7,9] and direct metal–metal bonding to form dimeric species [group 8 metal–OEP (OEP = octaethylporphyrin) complexes having the molecular formula $(OEPM)_2$ are known for M = Ru,[5] Os,[10] Ir,[11] and Rh[3,12]]. These characteristics have been attributed primarily to the increased π-bonding capabilities of the larger 4d and 5d orbitals of these metals over those of the smaller 3d orbitals of the first-row transition series.[6-8]

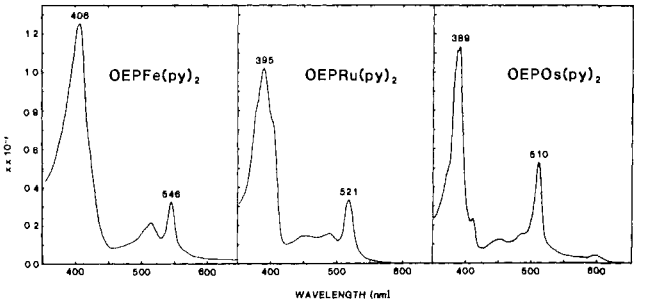

Figure 1. Electronic absorption spectra of (OEP)M(py)$_2$ in CH_2Cl_2 [Fe(II) and Ru(II)] and 3-methylpentane [Os(II)].

The heavy-metal group 8 porphyrins that have received the most attention are the monomeric Ru(II) and Os(II) complexes, which are homologues of the biologically important Fe(II) complexes. A systematic experimental and theoretical study of the electronic properties of Ru(II) and Os(II) porphyrins has been conducted by Gouterman, Buchler, and co-workers.[6-8] These workers observed a number of interesting features in the absorption spectra of the heavy-metal complexes, including hypso or blue-shifted Soret

(1) (a) Earl C. Anthony Fellow, 1981–1983. (b) Alfred P. Sloan Fellow, 1982–1984.

(2) (a) Drabkin, D. L. "The Porphyrins"; Dolphin, D., Ed.; Academic Press: New York, 1978; Vol. 1, pp 29–83. (b) Smith, K. M. "Porphyrins and Metalloporphyrins"; Smith, K. M., Ed.; Elsevier: Amsterdam, 1975; pp 3–28.

(3) Setsune, J.; Yoshida, Z.; Ogoshi, H. *J. Chem. Soc., Perkin Trans. 1*, **1982**, 983–987.

(4) (a) Holloway, C. E.; Stynes, D. V.; Vuik, C. P. J. *J. Chem. Soc., Dalton Trans.* **1982**, 95–101. (b) Sugimoto, H.; Mori, M. *Chem. Lett.* **1981**, 297–298. (c) Masuda, H.; Taga, T.; Osaki, K.; Sugimoto, H.; Mori, M.; Ogoshi, H. *J. Am. Chem. Soc.* **1981**, *103*, 2199–2203. (d) Domazetis, G.; James, B. R.; Dolphin, D. *Inorg. Chim. Acta* **1981**, *54*, L47–L49.

(5) Collman, J. P.; Barnes, C. E.; Collins, T. J.; Brothers, P. J. *J. Am. Chem. Soc.* **1981**, *103*, 7030–7032.

(6) Antipas, A.; Buchler, J. W.; Gouterman, M.; Smith, P. D. *J. Am. Chem. Soc.* **1980**, *102*, 198–207.

(7) Antipas, A.; Buchler, J. W.; Gouterman, M.; Smith, P. D. *J. Am. Chem. Soc.* **1978**, *100*, 3015–3024.

(8) Buchler, J. W.; Kokisch, W.; Smith, P. D. *Struct. Bonding (Berlin)* **1978**, *34*, 79–134.

(9) (a) Smith, P. D.; James, B. R.; Dolphin, D. *Coord. Chem. Rev.* **1981**, *39*, 31–75. (b) Buchler, J. W. "Porphyrins and Metalloporphyrins"; Smith, K. M., Ed.; Elsevier: Amsterdam, 1975; pp 157–232. (c) Tsutsui, M.; Taylor, G. A. *Ibid.* pp 279–313.

(10) Collman, J. P.; Barnes, C. E.; Woo, L. K.; Johnson, K. E. "Abstracts of Papers", 185th National Meeting of the American Chemical Society, 1983; American Chemical Society: Washington, D.C., 1983; INOR 0210.

(11) Wayland, B. B.; Woods, B. A.; Pierce, R.; Minda, V. M.; Duttahmed, A. 185th National Meeting of the American Chemical Society, 1983; American Chemical Society: Washington, D.C., 1983; INOR 0149.

(12) Ogoshi, H.; Setsune, J.; Yoshida, Z. *J. Am. Chem. Soc.* **1977**, *99*, 3869–3870.

0002-7863/84/1506-1682$01.50/0

and α (β) bands and prominent "extra" bands in the visible region of the spectrum. The hyspo spectral feature has been attributed to enhanced equatorial [metal(d_π) → porphyrin(π^*)] backbonding, which raises the energy of the porphyrin π^* orbitals. Certain of the "extra" bands in the visible spectrum have been assigned to allowed metal(d_π) → axial-ligand(π^*) charge-transfer (CT) transitions arising as a result of significant axial backbonding.[6] A number of bands observed in the visible spectra of Ru(II) and Os(II) porphyrins have also been attributed to low-lying doubly excited states [porphyrin($\pi \rightarrow \pi^*$) + metal(d_π) → porphyrin $(\pi^*)^{13}$] enhanced by equatorial backbonding.[7] The absorption spectra of the (OEP)Ru(py)$_2$ and (OEP)Os(py)$_2$ (py = pyridine) complexes (Figure 1) are particularly exemplary of the unusual features observed by Gouterman and Buchler in their studies of Ru(II) and Os(II) porphyrins. The spectra of the Ru(II) and Os(II) species exhibit prominent absorption bands around 400–450 nm in addition to the typical α, β, and Soret bands exhibited by the Fe(II) complex (Figure 1). The Os(II) complex also exhibits an absorption band near 600 nm, which is not observed for either the Fe(II) or Ru(II) complexes. The 400–450-nm bands have been attributed to doubly excited states,[7] while the 600-nm band remains unassigned. However, recent studies[14] of the Ru(II) complex alternatively assign the 450-nm band to a M(d_π) → py(π^*) CT transition analogous to that observed for bis(pyridine) adducts of iron(II) porphyrins.[14,15] Thus, the characterization of the electronic spectra of the heavy-metal complexes is by no means certain.

Resonance Raman (RR) spectroscopy is a sensitive probe for studying the structural and electronic properties of metalloporphyrin complexes.[16,17] Metalloporphyrins are particularly amenable to RR studies due to their strong visible and near-UV absorption characteristics, which give rise to extremely intense RR spectra. RR spectra of porphyrin complexes have been successfully interpreted in terms of theoretical models which incorporate vibronically induced scattering mechanisms.[18-21] In addition, specific frequency–structure correlations have been observed for a number of RR bands which correspond to particular vibrations of the porphyrin unit.[16] Thus RR spectroscopy can be used as a tool not only for the elucidation of vibronic activity for these complexes but for the determination of relative structural parameters as well. In view of the growing interest in Ru(II) and Os(II) porphyrins, RR spectral data should provide useful information for the complete characterization of their structural and electronic properties. As yet, however, no RR spectra have been reported for Os(II) porphyrin complexes, and only limited RR data are available for Ru(II) complexes.[14]

In this paper we present the results of a detailed RR study of a series of (OEP)M(py)$_2$ complexes in which M is Fe(II), Ru(II), or Os(II). We first present the RR data obtained with excitation throughout the visible region (405–630 nm). We next discuss in detail the metal–porphyrin system, considering the metal influences on both the vibrational frequencies and the RR excitation spectra. The RRES are used to better characterize the absorption spectra of, and vibronic coupling in, the complexes. We then consider the py–M–py systems of the (OEP)M(py)$_2$ complexes and discuss the implications of the observed frequency variations of bound-py vibrations in relation to axial-ligand bonding throughout the series.

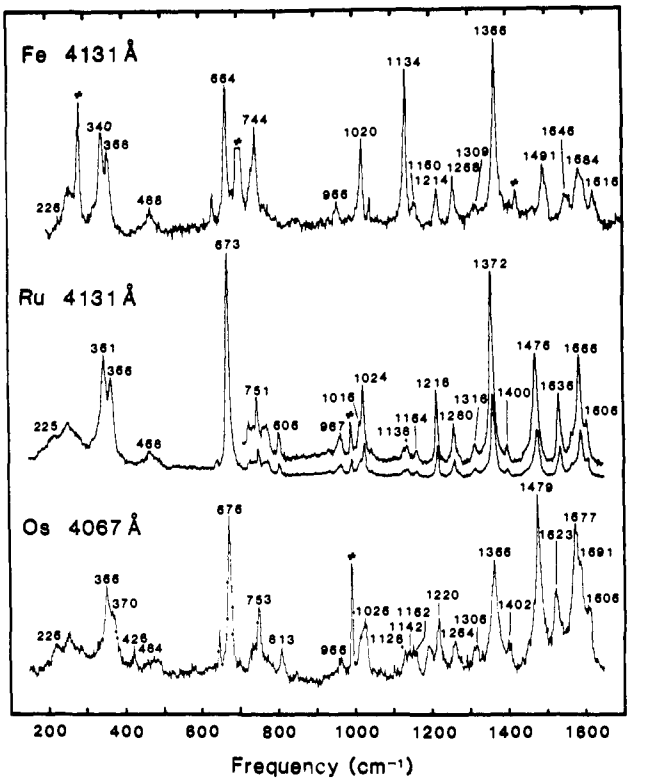

Figure 2. RR spectra of (OEP)M(py)$_2$ obtained with excitation in the vicinity of the B-state origins. ("#" is used to label bands due to solvent or internal standard.)

The py-mode RRES are used to characterize the electronic absorption bands in the visible region. Intensity measurements and fits of the RRES of the observed RR bands of the py ligands are also used to determine excited-state geometry displacements for these ligands.

II. Experimental Section

The (OEP)M(py)$_2$ complexes [M = Fe(II), Ru(II), and Os(II)] were prepared by following previously reported methods.[7,15,22] The identities of the prepared compounds were confirmed by their UV–vis absorptions. All solvents were spectral grade and were used without further purification.

The RR spectra were recorded in a 90% scattering configuration with use of the instrumentation and laser systems described earlier.[23] Excitation wavelengths were obtained by utilizing the tuning ranges of Stilbene 420, Coumarin 515, and Rhodamine 560 and 590 laser dyes (Exciton Chemical Co.). RR spectra of (OEP)Fe(py)$_2$ were obtained from an oxygen-free methylene chloride solution sealed in a glass capillary. The sample was maintained at 255 K by using a Harney–Miller cell to retard oxidation of Fe(II) to Fe(III). The Ru(II) and Os(II) complexes are air-stable in solid form (but unstable with respect to oxidation in methylene chloride, even at temperatures as low as 150 K) and were therefore suspended in compressed pellets with a supporting medium of sodium sulfate (1–2 mg of porphyrin to ~100 mg of sodium sulfate). The UV–vis absorption spectra of the Ru(II) and Os(II) complexes in the solid state (obtained from KBr and CsI pellets) are essentially identical with those obtained from solution. Spectra of the Os(II) sample were collected with the pellet spinning to avoid photodecomposition. All spectra were collected at either 1- or 2-cm^{-1} intervals (for frequency evaluation or intensity measurements, respectively) with integration times of 1–6 s/point as necesssary to produce respectable signal/noise. The spectral slit width was maintained at 4 cm^{-1} throughout the excitation region. Typical incident laser powers were 15 mW for the Fe(II) and Os(II) complexes and 30 mW for the Ru(II) complex. Sample integrity was continually monitored through the use of a multiscan averaging technique.

RRES were measured with respect to the 700-cm^{-1} band of methylene chloride in the case of the Fe(II) complex and with respect to the 994-

(13) (a) Kobayashi, H.; Hara, T.; Kaizu, Y. *Bull. Chem. Soc. Jpn.* **1972**, *45*, 2148–2155. (b) Kobayashi, H. *Adv. Biophys.* **1975**, *8*, 191–222. (c) Kobayashi, H.; Higuchi, T.; Eguchi, K. *Bull. Chem. Soc. Jpn.* **1976**, *49*, 457–463.

(14) Barrow, W. L., Ph.D. Thesis, Georgia Institute of Technology, 1982.

(15) Wright, P. G.; Stein, P.; Burke, J. M.; Spiro, T. G. *J. Am. Chem. Soc.* **1979**, *101*, 3531–3535.

(16) Spiro, T. G. "Iron Porphyrins"; Lever, A. B. P., Gray, H. B., Eds.; Addison-Wesley: Reading, MA, 1983; Part Two, pp 89–159.

(17) Felton, R. H.; Yu, N.-T. "The Porphyrins"; Dolphin, D., Ed.; Academic Press: New York, 1978; Vol. III, pp 347–393.

(18) Johnson, B. B.; Peticolas, W. *Annu. Rev. Phys. Chem.* **1976**, *27*, 465–491.

(19) Spiro, T. G.; Stein, P. *Annu. Rev. Phys. Chem.* **1977**, *28*, 501–521.

(20) Shelnutt, J. A.; Cheung, L. D.; Chang, R. C. C.; Yu, N.-T.; Felton, R. H. *J. Chem. Phys.* **1977**, *66*, 3387–3398.

(21) Shelnutt, J. A.; O'Shea, D. C. *J. Chem. Phys.* **1978**, *69*, 5361–5374.

(22) Buchler, J. W.; Smith, P. D. *Angew. Chem., Int. Ed. Engl.* **1974**, *13*, 341.

(23) Schick, G. A.; Bocian, D. F. *J. Am. Chem. Soc.* **1983**, *105*, 1830–1838.

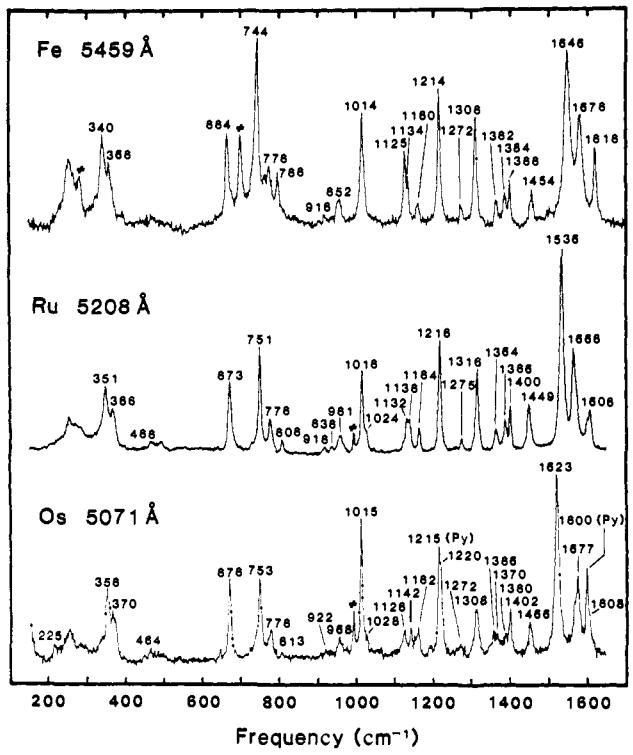

Figure 3. RR spectra of $(OEP)M(py)_2$ obtained with excitation near the Q-state origins. ("#" is used to label bands due to solvent or internal standard.)

cm^{-1} band of solid sulfate ion for the Ru(II) and Os(II) complexes. All profile points have been corrected for the ν^4 dependence of scattered light and instrument and photomultiplier responses. The RRES for $(OEP)Fe(py)_2$ obtained from a methylene chloride solution were corrected for reabsorption of the scattered light.[24] Reabsorption of the scattered light by the pellet samples was assumed to be negligible as a result of the scattering events occurring on or very near the surface of the pellets. [The validity of this assumption is substantiated by the fact that reabsorption-corrected RRES obtained for $(OEP)Ru(py)_2$ from a methylene chloride solution, although exhibiting a greater scatter of points due to slow thermally induced oxidation, appear identical with those obtained from the pellet sample.] Error bars representing 1 standard deviation above and below the corresponding points were determined for several excitation frequencies by multiple acquisition of the experimental points.

III. Results

A. Metalloporphyrin Skeletal Vibrations. RR spectra of the Fe(II), Ru(II), and Os(II) species of $(OEP)M(py)_2$ obtained with excitation near the Soret- and α-band maxima are shown in Figures 2 and 3, respectively. Frequencies observed for the RR bands of the Fe(II) complex are in reasonably good agreement with those previously reported for this species.[25] Generally, the RR spectra of the $(OEP)M(py)_2$ complexes are similar to those of other β-substituted metalloporphyrins.[16,17,25-31] The spectra appearing in Figure 3 are quite similar to one another, although the frequencies of several bands vary considerably (>10 cm^{-1}) with metal substitution. The spectra appearing in Figure 2 are somewhat dissimilar due to differences in excitation detuning from the B-state origins of the three complexes as governed by our laser tuning capabilities.

RR frequencies assignable to in-plane fundamental vibrations of the porphyrin skeleton are easily made by analogy to Ni(OEP)[26,32] and are given in Table I. Within experimental uncertainty, all depolarization ratios, ρ, are either 0.125, 0.75, or $\gg$1 and exhibit no apparent dispersions (with the exception of bands corresponding to more than one mode which are accidently nearly degenerate; see below). These values are those expected for a purely in-plane scattering mechanism for a system possessing 4-fold symmetry.[33] This allows a straightforward classification

Table I. Raman Frequencies (cm^{-1}) of the Fundamental In-Plane Porphyrin Skeletal Vibrations of $(OEP)M(py)_2$

assignment[a]		metal[b]			
sym	no.	Fe(II)	Ru(II)	Os(II)	P.E.D.[c]
A_{1g}	ν_2	1584	1586	1591	$\nu(C_\beta C_\beta) + \nu(C_\beta Et)$
	ν_3	1491	1476	1479	$\nu(C_\alpha C_m) + \nu(C_\alpha C_\beta)$
	ν_4	1366	1372	1365	$\nu(C_\alpha N) + \delta(C_\alpha C_m)$
	ν_5	1020	1024	1028	$\nu(C_\beta Et) + \nu(C_\alpha C_\beta)$
	ν_6	796	806	813	$\delta(C_\alpha C_m C_\alpha) + \nu(C_\alpha N)$
	ν_7	664	673	676	$\delta(C_\beta C_\alpha N) + \nu(C_\alpha C_\beta)$
	ν_8	340	351	356	$\delta(C_\beta Et) + \nu(C_\alpha C_m)$
	ν_9	~225	~225	~225	$\delta(C_\beta Et) + \nu(C_\alpha C_m)$
B_{1g}	ν_{10}	1618	1608	1608	$\nu(C_\alpha C_m) + \nu(C_\alpha C_\beta)$
	ν_{11}	1546	1535	1523	$\nu(C_\beta C_\beta) + \nu(C_\beta Et)$
	ν_{12}	1362	1364	1370	$\nu(C_\alpha N) + \nu(C_\beta C_\beta)$
	ν_{13}	1214	1218	1220	$\delta(C_m H) + \nu(C_\alpha C_\beta)$
	ν_{16}	744	751	753	$\delta(C_\alpha N C_\alpha) + \nu(C_\beta Et)$
A_{2g}	ν_{19}	1579	1566	1577	$\nu'(C_\alpha C_m) + \nu'(C_\alpha C_\beta)$
	ν_{20}	1384	1388	1390	$\nu'(C_\alpha N) + \nu'(C_\beta Et)$
	ν_{21}	1309	1316	1308	$\delta'(C_m H) + \nu'(C_\alpha C_\beta)$
	ν_{22}	1125	1132	1128	$\nu'(C_\alpha N) + \nu'(C_\beta Et)$
B_{2g}	ν_{28}	1454	1449	1455	$\nu'(C_\alpha C_m) + \nu'(C_\alpha C_\beta)$
	ν_{29}	1398	1400	1402	$\nu'(C_\alpha C_\beta) + \nu'(C_\beta Et)$
	ν_{30}	1160	1164	1162	$\nu'(C_\beta Et) + \nu'(C_\alpha N)$
	ν_{31}	1014	1016	1015	$\delta'(C_\alpha C_m) + \delta'(C_\alpha C_m C_\alpha)$
	ν_{32}	776	778	778	$\delta'(C_\beta Et) + \delta'(C_\alpha C_m)$
	ν_{35}	(179)[d]	(183)[d]	(185)[d]	$\delta'(C_\beta Et) + \delta'(C_\alpha C_m)$

[a] Number scheme follows that of Abe et al. (ref 32). [b] Frequencies for the Fe(II) complex were obtained from CH_2Cl_2 solutions. Frequencies for the Ru(II) and Os(II) complexes were obtained from Na_2SO_4 pellets. Frequencies obtained from CH_2Cl_2 solutions are within 2 cm^{-1} of those of the pellet. [c] The major internal-coordinate contributions to the normal modes as determined in ref 32. The symbols ν and δ (ν' and δ') denote stretching and bending symmetry coordinates which are symmetric (antisymmetric) about the C_2 axes of the pyrrole rings. [d] Not observed. The frequency shown is caluclated based on that of the observed first overtone.

Table II. Raman Frequencies (cm^{-1}) of Nonfundamental In-Plane Porphyrin Skeletal Vibrations of $(OEP)M(py)_2$

assignment[a]		metal[b]		
sym	no.	Fe(II)	Ru(II)	Os(II)
A_{1g}	$\nu_5 + \nu_9$	1258	1260	1264
	$\nu_6 + \nu_8$	1134	1138	1142
	$\nu_{32} + \nu_{35}$	956	967	968
	$2\nu_{35}$	358	366	370
B_{1g}	$\nu_{24} + \nu_{34}$	934	938	938
A_{2g}	$\nu_{16} + \nu_{35}$	916	919	922
B_{2g}	$\nu_9 + \nu_{31}$	1272	1275	1272
	$\nu_{18} + \nu_{24}$	952	961	958

[a] Number scheme follows that of Abe et al. (ref 32). [b] Frequencies for the Fe(II) complex were obtained from CH_2Cl_2 solutions. Frequencies for the Ru(II) and Os(II) complexes were obtained from Na_2SO_4 pellets. Frequencies obtained from CH_2Cl_2 solutions are within 2 cm^{-1} of those of the pellet.

(24) Strekas, T. C.; Adams, D. H.; Packer, A.; Spiro, T. G. *App. Spectrosc.* **1974**, *28*, 324-327.
(25) Kitagawa, T.; Teraoka, J. *Chem. Phys. Lett.* **1979**, *63*, 443-446.
(26) Kitagawa, T.; Abe, M.; Ogoshi, H. *J. Chem. Phys.* **1978**, *69*, 4516-4525.
(27) Spiro, T. G.; Burke, J. M. *J. Am. Chem. Soc.* **1976**, *98*, 5482-5489.
(28) Choi, S.; Spiro, T. G.; Langry, K. C.; Smith, K. M. *J. Am. Chem. Soc.* **1982**, *104*, 4337-4344.
(29) Choi, S.; Spiro, T. G.; Langry, K. C.; Smith, K. M.; Budd, D. L.; La Mar, G. N. *J. Am. Chem. Soc.* **1982**, *104*, 4345-4351.
(30) Spaulding, L. D.; Chang, C. C.; Yu, N.-T.; Felton, R. H. *J. Am. Chem. Soc.* **1975**, *97*, 2517-2525.
(31) Choi, S.; Spiro, T. G. *J. Am. Chem. Soc.* **1983**, *105*, 3683-3692.
(32) Abe, M.; Kitagawa, T.; Kyogoku, Y. *J. Chem. Phys.* **1978**, *69*, 4526-4534.

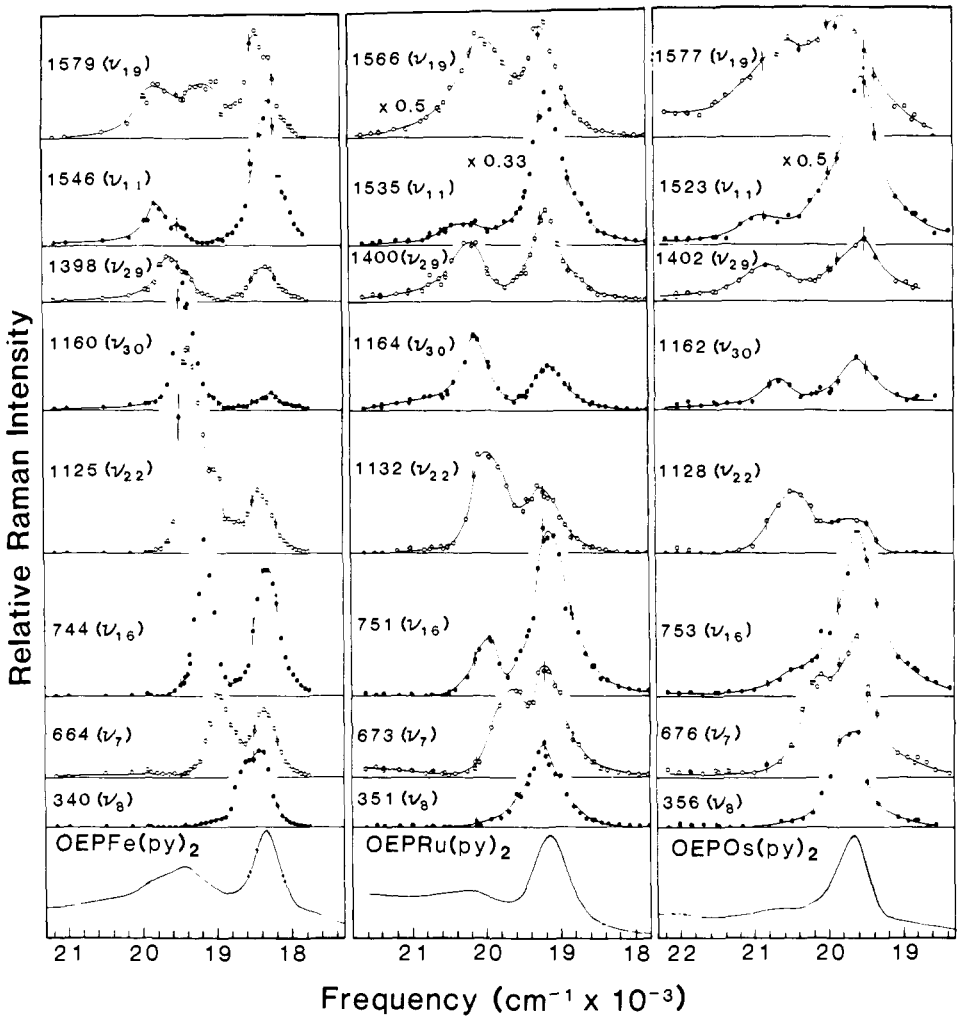

Figure 4. Q-state RRES for selected in-plane porphyrin skeletal modes of (OEP)M(py)$_2$ for M = Fe, Ru, and Os. The RRES are displaced vertically and are plotted using alternate filled (●) and open (○) circles for clarity. The solid curves are included only to facilitate viewing and do not represent calculated RRES. The spectra are identified by their corresponding RR frequencies and by their vibrational assignments (see Table I). The symmetry classifications for the displayed RRES are A_{1g} for ν_7 and ν_8, A_{2g} for ν_{19} and ν_{22}, B_{1g} for ν_{11} and ν_{16}, and B_{2g} for ν_{29} and ν_{30}. The absorption profiles for the Q-state regions are also shown for comparison. Error bars represent 1 standard deviation above and below the corresponding points based on repeated experimental measurements.

of the observed bands into their respective symmetries in the D_{4h} point group: A_{1g} ($\rho = 0.125$), A_{2g} ($\rho \gg 1$), and B_{1g} and B_{2g} ($\rho = 0.75$). Several overtone and combination bands are also observed and are listed in Table II. The frequencies of the nonfundamental modes correlate quite well with those observed in the RR spectra of other metalloporphyrins.[26,28,29] Several weak polarized bands are observed in the 400–500-cm^{-1} range which are not assignable to in-plane skeletal fundamental or nonfundamental vibrations. These bands are attributed to out-of-plane pyrrole folding and tilting modes analogous to those observed in the RR spectra of other metalloporphyrins.[31]

Q-state RRES for two representative fundamental porphyrin vibrations of each symmetry (ν_7 and ν_8, A_{1g}; ν_{19} and ν_{22}, A_{2g}; ν_{11} and ν_{16}, B_{1g}; and ν_{29} and ν_{30}, B_{2g}; see Table I) are shown in Figure 4 along with the corresponding absorption spectra. RRES were obtained from 630 to 405 nm for all three complexes. Resonance enhancement of the porphyrin skeletal vibrations is observed only with excitation into the Q and B states. No features are observed in the porphyrin-mode RRES that can be attributed to resonance enhancement via states between the Q and B states or to the red of the Q state for any of the three complexes.

For all three complexes, RRES of A_{1g} modes typically exhibit near-equal intensity in their Q(0,0) and Q(0,1) maxima. No particular trends are readily discernible upon substitution of the metal ion in the complexes. Similarly, the RRES of the A_{2g} modes do not exhibit trends as functions of metal substitution. However, certain of the A_{2g} modes do exhibit a variation in I_{0-1}/I_{0-0} in an inverse proportion to vibrational frequency. This effect is most dramatic in the Fe(II) complex (compare the RRES of ν_{19} and ν_{22} in Figure 4). The trend in I_{0-1}/I_{0-0} for the A_{2g} modes is accompanied by a tendency for the RRES of the higher frequency modes to exhibit broadened line widths and multiple vibronic peaks. For the Fe(II) complex additional features are observed in the form of shoulders near 700 cm^{-1} from Q(0,0).

The B_{1g} and B_{2g} bands of the (OEP)M(py)$_2$ series show significant trends in their RRES as functions of both vibrational frequency and metal substitution. For the Fe(II) complex, RRES of depolarized bands span a range from those that exhibit dominant Q(0,0) intensity, for example ν_{11} (1546 cm^{-1}) with $I_{0-1}/I_{0-0} \simeq 0.3$, to those that exhibit dominant Q(0,1) intensity, for example ν_{30} (1160 cm^{-1}) with $I_{0-1}/I_{0-0} \simeq 4$. Other modes, such as ν_{29} (1398 cm^{-1}), exhibit nearly equal Q(0,0) and Q(0,1) intensities. As the metal center is changed, I_{0-1}/I_{0-0} decreases in the order Fe > Ru > Os (compare the RRES of ν_{30} in Figure 4). As a consequence, RRES of the depolarized bands of the Ru(II) complex show either dominant Q(0,0) maxima or equal Q(0,0) and Q(0,1) intensity, and RRES of the depolarized bands of the Os(II) complex exhibit only dominant Q(0,0) maxima. In addition, the RRES of all depolarized bands of (OEP)Fe(py)$_2$ having frequencies above 1000 cm^{-1} exhibit weak shoulders near 1200 cm^{-1} from Q(0,0) as well as their respective Q(0,0) and Q(0,1) maxima. These features

(33) Bernstein, H. J. *Philos. Trans. R. Soc. London, Ser. A* **1979**, *293*, 287–302.

Table III. Observed and Calculated Frequencies (cm^{-1}) of the py Vibrations of $(OEP)M(py)_2$

		$(OEP)Fe(py)_2$		$(OEP)Ru(py)_2$		$(OEP)Os(py)_2$			$(OEP)Fe(py\text{-}d_5)_2$	
mode	py[a]	obsd[b]	calcd[c]	obsd[b]	calcd[c]	obsd[b]	calcd[c]	py-d_5	obsd[b]	calcd[c]
1	1580	1594	1603	1598	1603	1600	1603	1530	1553	1562
2	1482	*d*	1498	*d*	1499	*d*	1499	1340	1336	1362
3	1218	1214	1218	1215	1219	1215	1219	887	896	865
4	1068	*d*	1075	*d*	1079	*d*	1082	823	830	821
5	1029	1042	1036	1046	1040	1050	1043	1006	1020	1025
6	992	1006	1004	1014	1007	1015	1008	962	968	984
7	605	632	631	642	642	650	650	582	604	619
8		176	176	203	203	220	220		171	170

[a] Observed frequencies for py and py-d_5 taken from: Corrsin, L.; Fax, B. J.; Lord, R. C. *J. Chem. Phys.* **1953**, *21*, 1170–1176. [b] Frequencies for the Fe(II) complex were obtained from CH_2Cl_2 solutions. Frequencies for the Ru(II) and Os(II) complexes were obtained from Na_2SO_4 pellets. Frequencies obtained from CH_2Cl_2 solutions are within 2 cm^{-1} of those of the pellet. [c] Calculated by using the pyridine force field of ref 54. Metal-nitrogen stretching constants of 1.74, 2.48, and 3.08 mdyn/Å and $\nu(MN_{py})$-$\delta(C_1N_{py}C_1)$ interaction constants of −0.28, −0.43, and −0.55 mdyn Å were used for the Fe(II), Ru(II), and Os(II) complexes, respectively (see section IV.B.1). [d] Not observed.

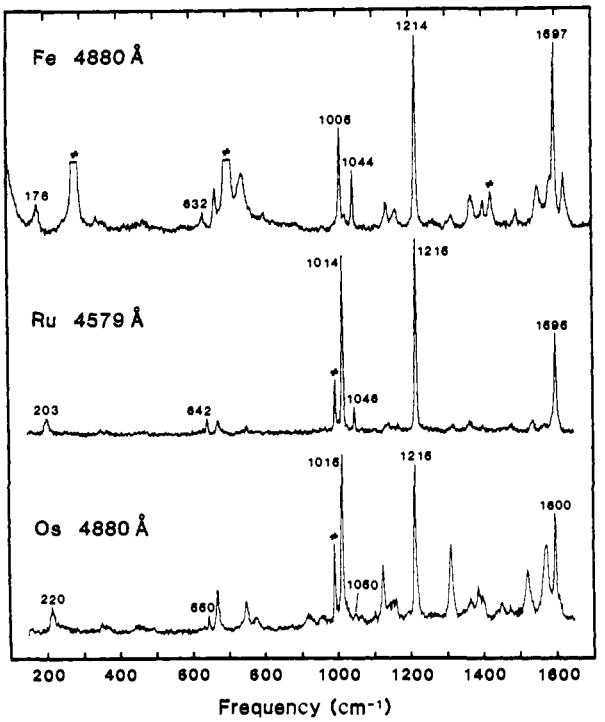

Figure 5. RR spectra of $(OEP)M(py)_2$ obtained with excitation between the B and Q states. ("#" is used to label bands due to solvent or internal standard.)

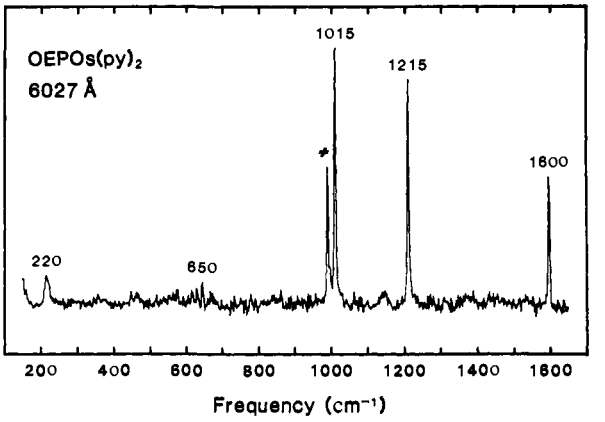

Figure 6. RR spectrum of $(OEP)Os(py)_2$ obtained with 6027-Å excitation. ("#" is used to label bands due to solvent or internal standard.)

are not observed for either of the Ru(II) and Os(II) complexes.

B. Pyridine Vibrations. With excitation between the Soret and α bands, a new set of RR bands due to resonance-enhanced totally symmetric vibrations of the py ligands[14,15,25] is observed in the spectra of all three complexes (Figure 5). No RR bands are observed above 1600 cm^{-1} which are assignable to combinations or overtones of these bands. The observed frequencies for the py modes of the Fe(II) and Ru(II) complexes are in good agreement with those previously reported.[14,25] The RR frequencies of the observed py modes of the three complexes are given in Table III along with those of free py. Also given in the table are the RR frequencies obtained for the py-d_5 species of the Fe(II) complex (spectrum not shown). The depolarization ratios for all bands are $\rho = 0.33$ and, with the exception of mode 3 of the Fe(II) complex and modes 3 and 6 of the Ru(II) complex, exhibit no dispersion. The latter three bands exhibit apparent polarization dispersions in which ρ varies from 0.33 (observed with excitation to the blue of the Q state) to 0.75 (observed with excitation to the red of the Q state). However, these py modes are coincident with strong depolarized porphyrin skeletal modes. Thus the dispersions represent only varying contributions from the porphyrin and py modes as functions of excitation frequency.

Excitation far to the red of the α-band maxima results in no apparent RR spectrum for either the Fe(II) or Ru(II) complex. However, for $(OEP)Os(py)_2$ excitation near the weak 600-nm absorption (Figure 1) results in a strong, exclusive enhancement of the py modes. A typical spectrum is shown in Figure 6. No additional bands are observed above 1600 cm^{-1}. The relative intensities of the bands are identical with those observed with excitation near 490 nm (compare Figures 5 and 6; the slight difference in the intensities shown in the figures is due to the fact that the spectrum obtained at 4880 Å is further from the band origin than that obtained at 6027 Å—see below). The depolarization ratios of the bands observed with excitation near 600 nm are all $\rho = 0.33$ and show no dispersion.

In order to determine the origin of the resonance enhancement observed for the py modes of the $(OEP)M(py)_2$ complexes, RRES of these modes were constructed for excitation wavelengths ranging from 405 to 630 nm. RRES observed for some of the stronger pyridine bands of the three complexes are shown in Figure 7 with the corresponding absorption spectra. The RRES of the Fe(II), Ru(II), and Os(II) complexes exhibit well-defined maxima near 19 800 cm^{-1} (505 nm), 21 450 cm^{-1} (466 nm), and 20 100 cm^{-1} (498 nm), respectively. [Note that the RRES of the Ru(II) complex also exhibit Q(0,0) and Q(0,1) maxima which are due to the intensity contributions of the coincident porphyrin modes.] These features and the observed depolarization ratios ($\rho = 0.33$) indicate that a *z*-polarized $M(d_\pi) \rightarrow py(\pi^*)$ CT transition (CTI) lies between the Q and B states for all three complexes. The energies of the CT transitions of the Fe(II) and Ru(II) complexes predicted by the detailed RRES reported here are in fair agreement with those estimated on the basis of earlier RR studies.[14,15] The RRES of all of the py modes of the Os(II) complex exhibit maxima coincident with the absorption maximum at 16 600 cm^{-1} (602 nm). Secondary maxima are also observed which are separated from the 602-nm maxima by approximately the ground-state frequencies of the respective py modes. These features indicate the presence of a second *z*-polarized $M(d_\pi) \rightarrow py(\pi^*)$ CT transition (CTII) near 602 nm. The secondary maxima in the RRES for this region correspond to 0–1 vibronic satellites of

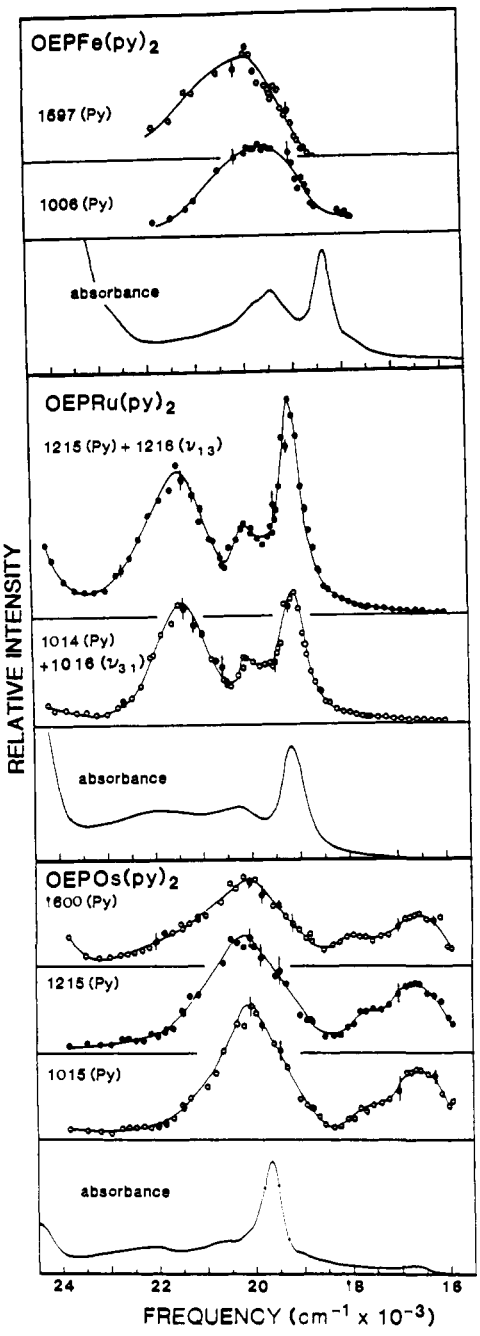

Figure 7. RRES for selected py modes of $(OEP)M(py)_2$. The RRES are displaced vertically and are plotted by using alternate filled (●) and open (○) circles for clarity. The solid curves are included only to facilitate viewing and do not represent calculated RRES. The spectra are identified by their corresponding RR frequencies (see Table III). The RRES labeled as the sum of two frequencies represent the intensity contributions of both the corresponding py mode and the nearly degenerate porphyrin skeletal mode. The absorption profiles for this region are also shown for comparison. Error bars represent 1 standard deviation above and below the corresponding point based on repeated experimental measurements.

the ~602-nm electronic origin. The energies of the $M(d_\pi) \rightarrow py(\pi^*)$ CT states of the $(OEP)M(py)_2$ complexes, along with those of the porphyrin B and Q states, are summarized in Table IV.

IV. Discussion

The observed RRES and depolarization ratios of the porphyrin and py RR bands of the $(OEP)M(py)_2$ complexes indicate that the porphyrin and py modes resonance enhance via different scattering mechanisms. The lack of interaction between the in-plane and out-of-plane scattering mechanisms is not totally unexpected. Kinematic coupling of the two systems should be small due to the orthogonality of the axially (py) and equatorially (porphyrin) directed motions of the nuclei. The π systems of the porphyrin and py ligands can interact through the metal d_π orbitals; however, the staggered configuration of the coplanar py ligands with respect to the porphyrin pyrrole nitrogens[34-37] should substantially reduce interactions via this pathway. In view of the apparent independence of the M–OEP and py–M–py systems of the $(OEP)M(py)_2$ complexes, we will examine each system separately in order to better characterize the effects of metal substitution on the equatorial and axial ligands.

Table IV. Electronic State Energies [cm^{-1} (nm)] for $(OEP)M(py)_2$

metal	$B(0,0)$ $(\pi\pi^*)$ [log ϵ]	CT1[a] $(d_\pi l_\pi^*)$ [log ϵ]	$Q(0,0)$ $(\pi\pi^*)$ [log ϵ]	CT11 $(d_\pi l_\pi^*)$ [log ϵ]
Fe(II)[b]	24600 (406) [5.10]	19450 (514) [3.5-3.75][c]	18300 (546) [4.41]	
Ru(II)[d]	25300 (395) [5.01]	21200 (472) [3.5-3.75][c]	19200 (521) [4.58]	
Os(II)[e]	25700 (389) [5.04]	19900 (503) [~3.70][f]	19600 (510) [4.71]	16550 (604) [~3.50]

[a] These numbers represent the electronic origins as determined by the RRES simulations (section IV.B.2.b). Note that the maxima in the RRES [505 nm (Fe), 466 nm (Ru), and 498 nm and 602 nm (Os)] do not correspond to the electronic origins. [b] Values for CH_2Cl_2 solution. [c] The extinction coefficients cannot be measured accurately due to overlapping absorption bands. The values are estimated based on the RR scattering from these states which is comparable to that of the Os(II) complex. [d] Values for benzene solutions. [e] Values for 3-methylpentane solutions. [f] Determined by the RRES simulations (section IV.B.2.b) based on the measured ϵ of CT11.

A. Metal–OEP System. 1. Vibrational Frequencies and Metal–OEP Interactions. The vibrational frequencies of metalloporphyrins are influenced by the metal center.[16,17] Metal properties such as bonding capabilities (σ and π), size, and charge are all important factors.[27,29,30,38-41] In the present series of $(OEP)M(py)_2$ complexes, certain RR bands systematically shift either to higher or to lower frequency with metal substitution, while others exhibit no systematic trends (Table I). These observations are indicative of a complex interplay of metal-related effects.

All bands having RR frequencies below 1100 cm^{-1} exhibit systematic upshifts with $\nu_{Fe} < \nu_{Ru} < \nu_{Os}$, with the exception of ν_{31} and ν_{32} (ν_9 does not appear to shift, but its frequency is poorly determined). In that the low-frequency modes should be the most sensitive to variations in the $M-N_{pyrrole}$ bonding these observations suggest that the increased σ-bonding capabilities of the metals across the series are responsible for the frequency variations of these modes. This was investigated by performing normal coordinate calculations on the metalloporphyrin skeleton. The modified Urey–Bradley force field determined by Abe et al.[32] was used, and the $M-N_{pyrrole}$ force constant was systematically increased. Altering the force constant by an amount commensurate with that expected for metal–nitrogen bonding (see Section IV.B.1) satisfactorily reproduces the upshifts in the frequencies of the A_{1g} and B_{1g} modes and the lack of shifts of the B_{2g} modes ν_{31} and ν_{32}. The B_{2g} (and A_{2g}) modes are not expected to shift, since these modes do not have the proper symmetry to mix with the $M-N_{pyrrole}$ stretches. It should be noted that the observed shift in the B_{2g}

(34) Hopf, F. R.; O'Brien, T. P.; Scheidt, W. R.; Whitten, D. G. *J. Am. Chem. Soc.* **1975**, *97*, 277–281.
(35) Bonnet, R.; Hursthouse, M. B.; Malik, K. M. A.; Mateen, B. *J. Chem. Soc., Perkin Trans. 2* **1977**, 2072–2076.
(36) Collins, D. M.; Countryman, R.; Hoard, J. L. *J. Am. Chem. Soc.* **1972**, *94*, 2066–2072.
(37) Radonovich, L. J.; Bloom, A.; Hoard, J. L. *J. Am. Chem. Soc.* **1972**, *94*, 2073–2078.
(38) Spiro, T. G.; Strekas, T. C. *J. Am. Chem. Soc.* **1974**, *96*, 338–345.
(39) Burke, J. M.; Kincaid, J. R.; Peters, S.; Gagne, R. R.; Collman, J. P.; Spiro, T. G. *J. Am. Chem. Soc.* **1978**, *100*, 6083–6088.
(40) Stong, J. D.; Spiro, T. G.; Kubaska, R. J.; Shupack, S. I. *J. Raman Spectrosc.* **1980**, *9*, 312–314.
(41) Shelnutt, J. A. *J. Am. Chem. Soc.* **1983**, *105*, 774–778.

mode ν_{35} is not predicted by the calculations; however, the frequency of this mode (Table I) is determined from the observed $2\nu_{35}$ band, which is in Fermi resonance with the A_{1g} mode ν_8.[31]

A number of bands with frequencies above 1100 cm^{-1}, particularly the B_{1g} modes, also show systematic shifts with metal substitution. The shifts observed in the B_{1g} modes of the three $(OEP)M(py)_2$ complexes correlate extremely well with the increase in M → porphyrin π-back-bonding which occurs across the series in the order Fe < Ru < Os. It has been suggested that B_{1g} modes should be particularly sensitive to back-bonding effects.[29] These motions are in-phase for equivalent bonds on opposite pyrroles and out-of-phase for these bonds on adjacent pyrroles. This phasing is the same as that of the nodal pattern on the porphyrin e_g (π^*) orbitals.[42] Examination of Table I reveals that modes ν_{10} and ν_{11}, which in general shift *down* across the series, involve atoms between which the bond order is lowered by e_g-orbital population. [The ν_{10} mode does not appear to shift upon substitution of Ru(II) by Os(II); however, this mode is also sensitive to other factors such as core size (see below).] Modes ν_{12} and ν_{13}, which shift *up*, involve bonds whose order is increased by e_g-orbital population.

All bands above 1450 cm^{-1}, with the exception of ν_2, exhibit downshifts in frequency upon substitution of Fe(II) by Ru(II). RR bands of metalloporphyrins in this frequency region are known to be sensitive to the size of the porphyrin core, an increased core size resulting in a lower frequency.[30] Substitution of Ru(II) for Fe(II) in $(OEP)M(py)_2$ results in a $M-N_{pyrrole}$ bond length increase from ~2.00 to ~2.05 Å.[34,37] The lowered frequencies for the Ru(II) complex are consistent with the increased core size. Substitution of Os(II) for Ru(II) does not, to any extent, expand the porphyrin core.[43] The frequencies of ν_3 and ν_{10} are essentially unchanged from the Ru(II) to the Os(II) complex, paralleling the core expansion across the series of metals Fe < Ru = Os. However, there are certain anomalies in the correlations of the core-size sensitive bands. The frequency of ν_2 increases across the series, and ν_{19} and ν_{28} occur a the same frequencies in the Os(II) and Fe(II) complexes. The origin of these anomalies is not clear.

Other bands, in addition to the core markers, exhibit anomalies upon substitution of the heavy metals into the porphyrin core. The frequencies of ν_4 and ν_{21} *increase* from Fe(II) to Ru(II) and *decrease* from Ru(II) to Os(II) such that $\nu_{Fe} \simeq \nu_{Os}$. The behavior of ν_4 is particularly curious. This mode is a well-known oxidation-state marker in iron porphyrins. Increasing M → porphyrin back-bonding lowers the frequency of this band. On this basis, it might be expected that the frequency of ν_4 in the $(OEP)M(py)_2$ complexes should systematically decrease across the series, $\nu_{Fe} > \nu_{Ru} > \nu_{Os}$. The fact that this is not observed indicates that other effects are important. In this regard, anomalous behavior of ν_4 in iron porphyrins has been interpreted in terms of an interplay of M → porphyrin back-bonding and effective metal nuclear charge. Increased backbonding reduces the frequency of ν_4 and increases the metal nuclear charge, which, in turn, partially compensates for the back-bonding effect.[29] Theoretical calculations on the $(OEP)M(py)_2$ complexes predict the metal nuclear charge to increase substantially from Fe(II) to Ru(II), but essentially not at all from Ru(II) to Os(II).[7] This effect could account for the increased frequency of ν_4 for the Ru(II) complex. The decrease in frequency of ν_4 with substitution of Os(II) for Ru(II) could be the result of the increased back-bonding capability of the former metal which predominates since the metal nuclear charge is nearly identical for these two heavy-metal complexes.

The anomalies in the frequencies of ν_4 and other metal-sensitive bands indicate that metal nuclear charge may be an important perturbation on the porphyrin π-electron system. Charge effects may contribute to σ-bonding, to polarization of the porphyrin π-orbitals, and to π-orbital delocalization.[41,44] The exact correlations of these metal-related effects await further RR studies on heavy-metal porphyrins.

2. Porphyrin $\pi\pi^*$ States and Vibronic Coupling Mechanisms. The intensities of the Q- and B-state absorptions of metalloporphyrins are influenced by Herzberg–Teller (HT) and Jahn-Teller (JT) coupling mechanisms.[45,46] For the $(OEP)M(py)_2$ complexes, the relative contributions of these mechanisms vary with metal substitution as is evidence by the variation in ϵ_Q/ϵ_B (Figure 1 and Table IV). RRES of porphyrin skeletal modes are extremely sensitive to the details of the vibronic activity.[20,21,47-50] In the following sections, we will examine the relative contributions of the various vibronic coupling mechanisms to the RRES of the porphyrin modes of the $(OEP)M(py)_2$ series.

a. General Features of the RRES. The RRES observed for the in-plane porphyrin skeletal modes of the $(OEP)M(py)_2$ series (Figure 4) exhibit features similar to those observed for other metalloporphyrins.[20,21,23,50-52] The observed features are characteristic of exclusive Q- and B-state scattering. As previously mentioned, there are no discernible contributions to the scattering tensors by additional states. In particular, bands attributed to doubly excited states appearing in the absorption spectrum of the Ru(II) and Os(II) complexes exhibit no RR scattering. Thus, the RR data lend no further insight into the nature of these states.

The RRES of the A_{1g} modes (ν_7 and ν_8; see Figure 4) are characterized by Q(0,0) and Q(0,1) maxima which are of nearly equal intensity and are drawn together by constructive interference (the constructive interference between the resonance terms governing the RRES of ν_8 has rendered the vibronic structure unresolved for this mode). These features are characteristic of dominant Franck–Condon (FC) scattering with little contribution from HT coupling.[53] Dominant FC scattering is generally not observed for A_{1g} modes of metalloporphyrins, but for the $(OEP)M(py)_2$ complexes it is undoubtedly due to the strong Q-state absorptions (Figure 1).

The RRES of the A_{2g} modes (ν_{19} and ν_{22}) exhibit Q(0,0)–Q(0,1) splittings which are substantially less than their ground-state frequencies. The constructive interference between Q(0,0) and Q(0,1) is expected for A_{2g} vibrations since these modes resonance-enhance via HT mechanisms.[47] The majority of A_{2g} modes for the Ru(II) and Os(II) complexes exhibit I_{0-1}/I_{0-0} of ~2 (note, for example, ν_{22} in Figure 4), which is indicative of weak HT coupling with nonadiabatic effects included.[21] Stronger vibronic coupling is observed for the Fe(II) complex as is evidenced by the extra features at ~700 cm^{-1} from Q(0,0) and by the deviations in I_{0-1}/I_{0-0} from the weak-coupling limit (particularly ν_{19}; Figure 4). The only evidence of strong coupling in the Ru(II) and Os(II) complexes is the approximate equality of I_{0-1} and I_{0-0} for ν_{19} (Figure 4). The stronger vibronic coupling in the Fe(II) complex is consistent with its smaller ϵ_Q/ϵ_B relative to that of the Ru(II) and Os(II) complexes.

The RRES of the B_{1g} (ν_{11} and ν_{16}) and B_{2g} (ν_{29} and ν_{30}) modes exhibit features indicative of both HT and JT activity. In the

(42) Gouterman, M. *J. Mol. Spectrosc.* **1961**, *6*, 138–163.
(43) Scheidt, W. R., private communication.
(44) Kitagawa, T.; Ogoshi, H.; Watanabe, E.; Yoshida, Z.-I. *J. Phys. Chem.* **1975**, *79*, 2629–2635.
(45) Gouterman, M. *J. Chem. Phys.* **1959**, *30*, 1139–1161.
(46) (a) Zerner, M.; Gouterman, M. *Theor. Chim. Acta* **1966**, *4*, 44–63. (b) Schaffer, A. M.; Gouterman, M. *Ibid.* **1970**, *18*, 1–13. (c) Sayer, P.; Gouterman, M.; Connell, C. R. *J. Am. Chem. Soc.* **1977**, *99*, 1082–1087.
(47) Friedman, J.; Hochstrasser, R. M. *Chem. Phys. Lett.* **1975**, *32*, 414–419.
(48) Zgierski, M. Z.; Shelnutt, J. A.; Pawlikowski, M. *Chem. Phys. Lett.* **1979**, *68*, 262–266.
(49) Shelnutt, J. A.; Yu, N.-T.; Chang, R. C. C.; Cheung, L. D.; Felton, R. H. "Proceedings of the Fifth International Conference on Raman Spectroscopy"; Schmid, E.; Brandmuller, J.; Kiefer, W.; Schrader, B.; Schrotter, H., Eds.; Schulz; Freiburg, 1976; pp 336–337.
(50) (a) Verma, A. L.; Bernstein, H. J. *J. Chem. Phys.* **1974**, *61*, 2560–2565. (a) Verma, A. L.; Mendelson, R.; Bernstein, H. J. *Ibid.* **1974**, *61*, 383–390. (c) Mendelson, R.; Sunder, S.; Verma, A. L.; Bernstein, H. J. *Ibid.* **1975**, *62*, 37–44. (d) Sunder, S.; Mendelson, R.; Bernstein, H. J. *Ibid.* **1975**, *63*, 573–580.
(51) (a) Spiro, T. G.; Strekas, T. C. *Proc. Natl. Acad. Sci. U.S.A.* **1972**, *69*, 2662–22. (b) Strekas, T. C.; Spiro, T. G. *J. Raman Spectrosc.* **1973**, *1*, 387–392.
(52) Chang, R. C. C. Ph.D. Thesis, Georgia Institute of Technology, 1976.
(53) Shelnutt, J. A. *J. Chem. Phys.* **1981**, *74*, 6644–6657.

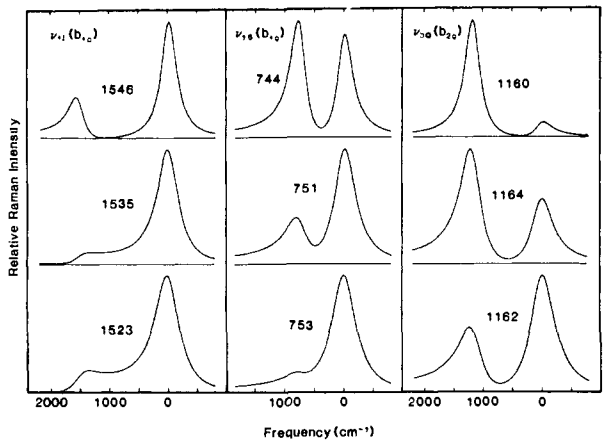

Figure 8. Simulated Q-state RRES for the in-plane porphyrin skeletal modes ν_{11}, ν_{16}, and ν_{30} of (OEP)M(py)$_2$ where M = Fe(II) (top), Ru(II) (middle), and Os(II) (bottom). The corresponding RR frequencies are given in cm^{-1}. The frequency axis is labeled in Δcm^{-1} from the respective Q-state origins (Table IV) to facilitate comparison. All RRES have been normalized to produce the same absolute intensity maxima. The parameters used in the simulations (see Appendix) for the Fe(II), Ru(II), and Os(II) complexes are, respectively, θ = 24°, 31°, and 34°; $\Gamma_Q = \Gamma_B$ = 160, 220, and 250 cm^{-1}; b_g/b_g' = 1.7, 2.2, and 2.0 for ν_{11}, 0.90, 0.67, and 0.61 for ν_{16}, and 0.67, 0.55, and 0.55 for ν_{30}.

weak (HT) coupling limit, B_{1g}- and B_{2g}-mode RRES are expected to exhibit $I_{0-1}/I_{0-0} \simeq 2$ with the Q(0,0) and Q(0,1) maxima separated by the respective ground-state frequencies. JT activity induced by CI "unmixing" of the Q and B states (from their 50/50 excited-state configuration mixtures as defined by Gouterman's four-orbital mode[45]) results in deviations in I_{0-1}/I_{0-0} from the HT limit.[20] Certain RRES of the (OEP)M(py)$_2$ series [particularly those of the two B_{1g} modes of the Os(II) complex; Figure 4] exhibit constructive interference between Q(0,0) and Q(0,1) resonances. This is indicative of large values of the CI parameter which introduces significant JT activity and reverses the sign of interfering vibronic cross terms.[53] If only CI-induced JT activity is present in the (OEP)M(py)$_2$ complexes, the RRES of the depolarized modes would, for a given complex, all appear similar, with I_{0-1}/I_{0-0} varying slightly and smoothly as a function of vibrational frequency.[53] This simple behavior is not observed, indicating that *intrinsic* JT activity is present in the Q-state and that the four-orbital model is not strictly valid.[48,49] For example, $I_{0-1}/I_{0-0} \simeq$ 6 for ν_{30} of the Fe(II) complex (Figure 4) is due to interference between intrinsic and CI-induced JT contributions. The RRES of the Fe(II) complex are further complicated by deviations from the weak-coupling limit as is evidenced by the shoulders in the RRES at $\sim$1200 cm^{-1}. Despite these complications for the Fe(II) complex, the general trend in I_{0-1}/I_{0-0} for a given mode of the three (OEP)M(py)$_2$ complexes is a decrease in the order Fe > Ru > Os, consistent with increasing JT activity induced by increases in the CI parameter for the series.

b. Calculated RRES. Metal substitution in the (OEP)M(py)$_2$ series greatly influences the extent of CI between the Q and B states, altering the vibronic coupling of the various vibrations of the porphyrin skeleton. This effect is quite important for the B_{1g} and B_{2g} modes but is not important for the A_{1g} modes since the RRES of the latter are determined primarily by FC scattering. In order to quantitate the trends in the RRES of the B_{1g} and B_{2g} modes, we have modeled the RRES utilizing the methods previously outlined by Shelnutt.[53] A brief description of the model as applied in this case is given in the Appendix. This simple method is based on a single-mode approximation; therefore, features in the RRES arising from strong-coupling effects are not considered. Strong-coupling effects are, for the most part, absent in the RRES of the Ru(II) and Os(II) complexes but are present in those of the Fe(II) complex. However, vibronic coupling involving the B_{1g} and B_{2g} modes of the latter complex is still comparatively weak;[20,21] thus the simple model should still provide a reasonable estimate of the relative vibronic contributions. It should also be noted that the observed variations in the shapes of the A_{2g} RRES cannot be modeled by this method since I_{0-1}/I_{0-0} is predicted to be independent of the CI parameter for modes of this symmetry.[53]

Calculated RRES for ν_{11} (B_{1g}, ca. 1530 cm^{-1}), ν_{16} (B_{1g}, ca. 750 cm^{-1}), and ν_{30} (B_{2g}, ca. 1160 cm^{-1}) are shown in Figure 8. The RRES were calculated by using eq A-5 and A-6. Four parameters are needed for the simulations: θ, the CI parameter; b_g' and b_g'', the intrinsic JT coupling in the zero-order Q and B states; and b_g, the zero-order HT coupling. The inclusion of the b_g' and b_g'' terms is necessary to model the profiles, reflecting the breakdown of the simple four-orbital model. Consequently, the CI parameter (θ) cannot be interpreted in the same fashion as is predicted by the simple model (see Appendix). The CI parameters were estimated from the absorption spectra with $\theta \simeq \tan^{-1}[(f_Q\nu_B/f_B\nu_Q)^{1/2}]$.[20] This yields θ_{Fe} = 24°, θ_{Ru} = 31°, and θ_{Os} = 34°. The vibronic coupling parameters were then varied to fit the RRES. Only relative values of the coupling parameters can be determined since absolute intensities were not measured. [Every coupling-dependent term (eq A-6) is linear; therefore changing the magnitudes of b_g, b_g', and b_g'' is equivalent to using a scaling factor.]

The intensities of the RR bands of the three (OEP)M(py)$_2$ complexes drop to nearly zero in the excitation region to the blue of the Q state (Figure 4), indicating destructive interference in this region. For the Fe(II) complex, destructive interference is also observed between Q(0,0) and Q(0,1). In order to account for these observations, b_g/b_g' must be positive and b_g''/b_g' must be negative. The simulations also indicate that $|b_g''/b_g'|$ must be at least unity to account for the lack of scattering intensity between the Q and B states; therefore $b_g''/b_g' = -1$ is used for all simulations.

The RRES of ν_{11}, ν_{16}, and ν_{30} of the Fe(II) complex are reasonably simulated with b_g/b_g' of $\sim$1.7, $\sim$0.90, and $\sim$0.67, respectively. The RRES for the Ru(II) and Os(II) complexes are simulated in reasonably good agreement with those observed by using these values and changing only θ. The simulations correctly predict the introduction of constructive interference between Q(0,0) and Q(0,1) for ν_{16} of the Os(II) complex and for ν_{11} of both the Ru(II) and Os(II) complexes. Essentially perfect fits can be obtained for the RRES of the Ru(II) and Os(II) complexes if b_g/b_g' is allowed to vary. The best values for the Ru(II) and Os(II) complexes were found to be 2.2 and 2.0 for ν_{11}, 0.67 and 0.61 for ν_{16}, and 0.55 and 0.55 for ν_{30}, respectively.

In summary, the calculations indicate that metal substitution in the (OEP)M(py)$_2$ series alters not only the CI between the Q and B states (θ) but also the relative zero-order vibronic activities (b_g/b_g') of the B_{1g} and B_{2g} porphyrin skeletal modes. However, the variation in the CI is the dominant factor contributing to the trends in the RRES.

B. Py–Metal–Py System. 1. Vibrational Frequencies and Metal–Py Bonding. Several of the resonance-enhanced py modes of the (OEP)M(py)$_2$ series are substantially different from those of the corresponding modes of free py (Table III). In general, the frequencies of the bound py modes are higher than those of free py and exhibit upshifts upon metal substitution in the order $\nu_{Fe} < \nu_{Ru} < \nu_{Os}$. It is not obvious whether these upshifts are due to kinematic effects or to alterations in the force field of the py ring via σ- and/or π-bonding to the metal. In this regard, recent normal coordinate calculations for non-porphyrin metal–py complexes reported by Suzuki and Orville-Thomas[54] indicate that the observed shifts in the py frequencies upon metal coordination are caused mainly by kinematic mixing of the metal–py stretch with the internal modes of the py ligand and that the py force field is essentially unaltered. In order to better determine how metal substitution in the (OEP)M(py)$_2$ complexes influences the vibrational frequencies of the py ligands, we have performed a normal mode analysis on the py–M–py system.

The normal coordinate calculations were performed on the py–M–py system by using the py geometry of Bak et al.[55] with

(54) Suzuki, S.; Orville-Thomas, W. J. *J. Mol. Struct.* **1977**, *37*, 321–327.

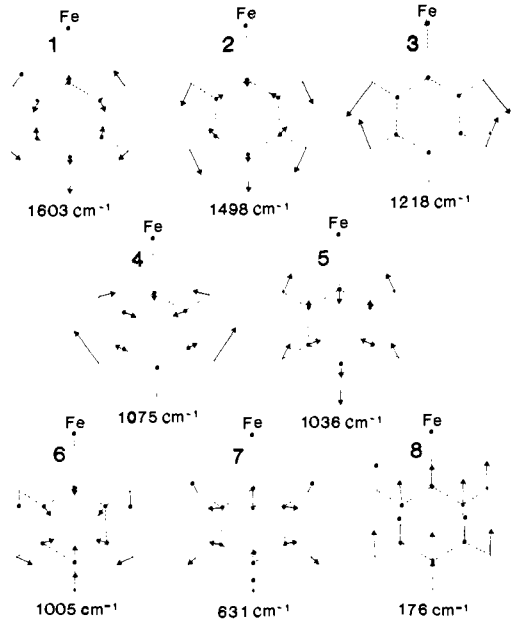

Figure 9. Eigenvectors of the A_{1g} modes of the py–Fe–py system. Only half of the system is shown for clariy. The eigenvectors shown all represent positive phasing as defined for the excited-state origin shift analysis (see the text).

a M–N_{py} bond length of 2.05 Å, which was for simplicity taken to be the same for all three complexes of the (OEP)M(py)$_2$ series [changes of up to 5% in the bond lengths and bond angles of the M–py system do not significantly alter the calculated potential energy distribution (<2%) or vibrational frequencies (<1 cm^{-1})]. The modified Urey–Bradley force field of Suzuki and Orville-Thomas[54] for py was used, neglecting potential-energy coupling between the two bound py ligands since satisfactory results are obtained without inclusion of such interaction terms. A M–N_{py} stretch constant (F_r) and a non-Urey–Bradley stretch (M–N_{py})–bend (C_1NC_1) interaction constant ($F_{r\alpha}$) were added to the force field. The $F_{r\alpha}$ influences the calculated frequencies of only modes 7 and 8 and is necessary in order to reproduce the frequency shifts observed for mode 7. The values of the force constants determined by the calculations are F_r = 1.74, 2.48, and 3.08 mdyn/Å and $R_{r\alpha}$ = −0.28, −0.43, and −0.55 mdyn/rad for the Fe(II), Ru(II), and Os(II) systems, respectively. The frequencies calculated by using this force field for py bound to Fe(II), Ru(II), and Os(II), and for py-d_5 bound to Fe(II), are compared in Table III to those observed. Eigenvectors for the in-plane A_{1g} modes of the py–Fe–py system are shown in Figure 9. Only half of the system is shown for clarity.

The frequency upshifts that occur upon metal–py binding for both the h_5 and d_5 species are well reproduced by the calculations. A majority of the frequency trends occurring upon metal substitution are also well reproduced by the calculations. These results indicate that kinematic mixing of the M–N_{py} stretch with the internal modes of the bound py ligands is primarily responsible for the observed frequency upshifts, although changes in the σ-bonding capabilities of the metal (Fe < Ru < Os) also influence the frequencies of the bound py ligand through $F_{r\alpha}$. There are, however, metal-dependent trends in the frequencies of certain modes (1 and 6) that are not completely accounted for by the calculations. This may reflect changes in the electronic structure of the py ligands due to alterations in the back-bonding capabilities of the metal center. This possibility is supported by the calculated compositions of the normal modes (Figure 9). Modes 3, 5, and 7, for which the frequency trends are well predicted, are all primarily bending modes, whereas modes 1 and 6, for which the trends are not as well predicted, are primarily ring stretching vibrations. These latter modes should be the most sensitive to changes in the py π-density due to back-bonding from the coordinated metal.

2. Metal–Py CT and Excited-State Geometries. a. Characterization of the Absorption Spectra. The RRES of the py modes of the (OEP)M(py)$_2$ complexes (Figure 7) indicate that z-polarized M(d_π) → py(π^*) CT absorptions occur at 514, 472, and 503 nm for the Fe(II), Ru(II), and Os(II) species, respectively (Table IV). The ordering observed for the CTI states of the three complexes is consistent with the calculated d_π-orbital energy ordering of the metal ions, Ru(II) < Fe(II) ≃ Os(II) (the energy of the py π^* orbitals is essentially metal independent).[7] It is interesting that the CTI states of the Ru(II) and Os(II) complexes occur at very different energies. An absorption maximum occurs in the spectra of both complexes around 450 nm (Figure 1), which Gouterman and Buchler[8] originally assigned to a transition to a doubly excited state. Alternatively, Barrow[14] has assigned the 450-nm band of the Ru(II) complex to a M(d_π) → py(π^*) CT transition. The results of our RR studies indicate that the 450-nm band of the Os(II) complex *does not* correspond to a M(d_π) → py(π^*) CT transition, while such an absorption does contribute to this region of the spectrum of the Ru(II) complex. This suggests that the 450-nm absorption of *both* complexes may contain contributions from doubly excited states as was originally proposed.

The RRES of the py modes of (OEP)Os(py)$_2$ indicate that a second M(d_π) → py(π^*) CT absorption occurs at 604 nm. The relative resonance enhancements of the py modes of the Os(II) complex observed with excitation into CTII are virtually identical with those observed with excitation into CTI, indicating that the two CT states in the Os(II) complex involve the *same* π^* orbitals of the py ligands. The occurrence of the two CT absorptions in the spectrum of the Os(II) complex is attributed to the large spin–orbit coupling of the metal ion ($\lambda_{Os} \simeq 3000$ cm^{-1} compared to $\lambda_{Ru} \simeq 1000$ cm^{-1} and $\lambda_{Fe} \simeq 400$ cm^{-1}).[56] Promotion of an electron from the metal d_π orbitals to the py ligands results in a $(t_{2g})^5$ configuration for the metal ion. Spin–orbit coupling splits this configuration into two states with total angular momenta of $j = {}^1/_2$ and $j = {}^3/_2$ separated by $3\lambda/2$[57] (the ligand field of the porphyrin system is actually tetragonal, which splits the $j = {}^3/_2$ states into two Kramers doublets; however, this splitting is small compared to the spin–orbit interaction[7]). The splitting between CTI and CTII in the Os(II) complex is 3500 cm^{-1} (Table IV), predicting a spin–orbit interaction of ~2300 cm^{-1}, similar to that observed in Os(III) complexes.[58] In that the two CT absorptions of (OEP)Os(py)$_2$ are due to metal-centered excited-state effects, it is not surprising that the relative resonance enhancements of the py modes observed with excitation into these two states are identical.

b. Calculated Excited-State Geometry Displacements. Resonance-enhanced Raman intensities can be used to obtain excited-state geometry displacements.[59-62] In this regard, Spiro and co-workers used the observed relative intensities of the resonance-enhanced py modes of (MP)Fe(py)$_2$ (MP = mesoporphyrin IX dimethyl ester) to determine the CT excited-state displacements for the py–M_λ–py system.[15] However, the RRES obtained for the py modes of (MP)Fe(py)$_2$ were limited (five excitation wavelengths) and no vibronic structure could be resolved. Consequently, only *relative* values for excited-state displacements of the various modes could be determined. In order to obtain values for the displacements, Spiro and co-workers assumed a linear relationship

(55) Bak, B.; Hansen-Nygaard, L.; Rastrup-Andersen, J. *J. Mol. Spectrosc.* **1958**, *2*, 361–368.

(56) (a) Goodman, B. A.; Raynor, J. B. *Adv. Inorg. Chem. Radiochem.* **1970**, *13*, 192. (b) Figgis, B. N.; Lewis, J. *Prog. Inorg. Chem.* **1964**, *6*, 99. (c) Dunn, T. M. *Trans. Faraday Soc.* **1961**, *57*, 1441–1444.

(57) Ballhausen, C. J. "Introduction to Ligand Field Theory"; McGraw-Hill: New York, 1962; p 119.

(58) (a) Hill, H. J. *J. Chem. Soc., Faraday Trans. 2* **1972**, *68*, 427–434. (b) Hudson, A.; Kennedy, M. J. *J. Chem. Soc. A* **1969**, 1116–1120.

(59) (a) Warshel, A. *Annu. Rev. Biophys. Bioeng.* **1977**, *6*, 273–300. (b) Warshel, A.; Karplus, M. *J. Am. Chem. Soc.* **1974**, *96*, 5677–5689.

(60) Blazej, D. C.; Peticolas, W. L. *Proc. Natl. Acad. Sci. U.S.A.* **1977**, *74*, 2639–2643.

(61) Peticolas, W. L.; Blazej, D. C. *Chem. Phys. Lett.* **1979**, *63*, 604–608.

(62) Blazej, D. C.; Peticolas, W. L. *J. Chem. Phys.* **1980**, *72*, 3134–3142.

Table V. Intensities and Excited-State Normal-Mode Displacements for the py Vibrations of (OEP)M(py)$_2$

	(OEP)Fe(py)$_2$		(OEP)Ru(py)$_2$		(OEP)Os(py)$_2$		(OEP)Fe(py-d_5)$_2$		
mode	I_{obsd}[a]	Δ_s[b]	I_{obsd}[a]	Δ_s[b]	I_{obsd}[a]	Δ_s[b]	I_{obsd}[a]	I_{calcd}[c]	Δ_s[b]
1	(1.0)	0.53	(1.0)	0.46	(1.0)	0.57	(1.0)	(1.0)	0.63
2		0.0		0.0		0.0	0.07	0.01	0.06
3	1.1	0.60	1.6	0.63	1.3	0.67	0.25	0.27	0.42
4		0.0		0.0		0.0	0.06	0.08	0.24
5	0.28	0.34	0.13	0.20	0.07	0.17	0.07	0.03	0.14
6	0.67	0.51	1.3	0.60	1.4	0.68	1.07	0.81	0.65
7	0.04	0.19	0.08	0.21	0.13	0.27	0.04	0.04	0.21
8	0.06	0.44	0.11	0.47	0.11	0.49	0.05	0.04	0.44

[a] Observed intensities obtained with excitation at the electronic origin of CTI and normalized to the intensity of mode 1. The intensities were measured from CH_2Cl_2 solutions (Fe and Ru) and Na_2SO_4 pellets (Ru and Os). [b] Excited-state origin displacements (dimensionless) determined by fitting the RRES (see section IV.B.2.b). [c] Δ_S values calculated from cartesian displacements determined for py-h_5 species by using phasing of +, +, −, −, −, + for modes 1, 3, 5, 6, 7, 8, respectively. I_{calcd} represent the intensities calculated from Δ_S by using eq B-1 and B-2 (see Appendix).

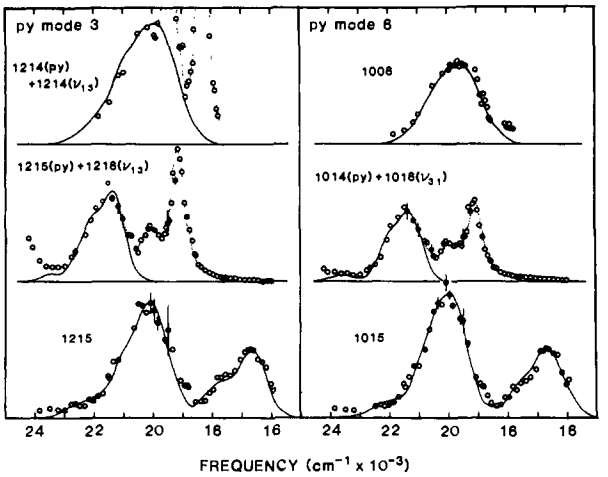

Figure 10. Comparison of observed (circles) and calculated (solid curves) RRES for py modes 3 and 6 of the (OEP)M(py)$_2$ complexes of Fe(II) (top), Ru(II) (middle), and Os(II) (bottom). The corresponding RR frequencies are given in cm^{-1}. The RRES are normalized to the stronger of the bands for each complex. The calculations were performed by using the electronic origins given in Table IV, the Δ_s values in Table V, and the method outlined in Appendix B. Homogeneous line widths of 250 cm^{-1} for CTI and 125 cm^{-1} for CTII were used with an inhomogeneous Gaussian spectral broadening of 350 cm^{-1}. Mode 3 of (OEP)Fe(py)$_2$ and modes 3 and 6 of (OEP)Ru(py)$_2$ are nearly coincident with in-plane porphyrin skeletal modes. The RRES of these latter modes are labeled as sums of the corresponding RR frequencies. The dotted lines appearing in the RRES represent the porphyrin-mode intensity contributions which were not included in the simulations.

between the FC factors and origin shifts and scaled their calculations using geometrical parameters predicted by MO calculations. The detailed profiles we report here for the (OEP)M(py)$_2$ complexes allow a more quantitative determination of the excited-state origin shifts. Vibronic structure is clearly observed in the RRES of the py modes of (OEP)Os(py)$_2$ with excitation into CTII. Also, evidence of vibronic structure is seen in the RRES near the CTI maxima for all three complexes. This is most apparent for the Fe(II) and Os(II) complexes, which exhibit a definite skewing toward the high-energy side.

The origin shifts, Δ_s, for the py modes of (OEP)Os(py)$_2$ were determined by fitting the RRES from 430 to 650 nm using eq B-1 and B-2 (Appendix). These Δ_s values are given in Table V. Representative simulated RRES are shown in Figure 10. The simulations were performed by first estimating Δ_s for each mode using a single-mode approximation for the scattering tensor. These Δ_s values were then used in the complete multimode expression (eq B-1) to simulate the RRES and were optimized to produce the best fit for each mode. It was found that multimode effects were adequately accounted for by including only the three lowest vibrational states for each mode. The simulations indicate that the Δ_s values which give the best fits to the RRES in the region of CTII also give reasonable fits in the region of CTI. However, the uncertainties in the Δ_s values for CTI are larger since the vibronic structure in the RRES for this region is poorly resolved. The RRES for the py modes of the Ru(II) and Fe(II) complexes were fit in a fashion similar to that described for the Os(II) complex. The Δ_s values determined for the py modes of the latter complex were taken as initial values for the calculations. The optimized Δ_s values for the Fe(II) and Ru(II) complexes are given in Table V. Representative simulated RRES are shown in Figure 10.

Table VI. Excited-State Bond Length Displacements of the Py-M-Py Systems of (OEP)M(py)$_2$

	origin shift[a]		
bond	Fe(II)	Ru(II)	Os(II)
M-N	−19 (12)[b]	−17 (10)[b]	−19 (12)[b]
N-C_1	20 (1)	17 (2)	19 (3)
C_1-C_2	−10 (2)	−9 (2)	−11 (3)
C_2-C_3	18 (1)	21 (1)	23 (2)

[a] Defined as $\delta r = r_{ex} - r_{gr}$ where r_{ex} and r_{gr} are the coordinate values for the excited and ground states, respectively. Given in units of 0.001 Å. [b] Average values (standard deviations) of those determined by using the three normal mode phase solutions (see section IV.B.2.b).

After determination of the Δ_s values, the excited-state geometry displacements were calculated by using eq B-3 (Appendix). Since the origin shifts are determined by the square roots of the intensities, the signs of Δ_s are not experimentally determinable. Consequently, there are 2^m possible phase combinations for a set of m values of Δ_s, giving 2^m different excited-state geometries. Constraints can be placed on the calculation based on the nodal pattern of the py π^* orbital involved in the CT transition. The nodal planes of the π^* orbital pass through the N-C_1 and C_2-C_3 bonds; consequently, the promotion of an electron to the py π^* orbital is expected to result in an excited state for which the internal coordinate displacements show a decrease in the C_1-C_2 bond length and increase in the N-C_1 and C_2-C_3 bond lengths. The CT transition is also expected to induce a decrease in the M-N_{py} bond length as a result of the increase in electrostatic attraction between the negative py ligands and the positive metal ion. Only seven of the possible phase combinations for Δ_s values give consistent results for the entire series of complexes by using the above expected displacement directions. These seven solutions can further be reduced by reversing the intensity calculation to predict the RR intensities for the py-d_5 complexes.[15] A comparison of the observed intensities of (OEP)Fe(py)$_2$ (Table V) to those predicted by the seven remaining combinations yields three solutions which give reasonable consistency between calculations and experiment. The three differ only in the phases of modes 7 and 8. All three predict positive phasing for modes 1 and 3 and negative phasing for modes 5 and 6 (the eigenvectors drawn in Figure 9 all represent the positive phases). For modes 7 and 8 the respective phasing is predicted to be negative and positive by solution 1, both positive by solution 2, and both negative by solution 3. The results of the intensity calculation using solution 1 are

shown in Table V. Solutions 2 and 3 give identical intensities to within 0.01.

Excited-state coordinate displacements calculated by using the above methods for the bound py ligands of the $(OEP)M(py)_2$ complexes are given in Table VI. The values appearing in the table represent the averages of those calculated by using the three phase combinations determined above. All three solutions give nearly equal values for all bond displacements except $\delta r(MN_{py})$ as can be seen by the standard deviations. The disparity in the $M-N_{py}$ displacement is expected in that modes 7 and 8 are calculated to be responsible for nearly 50% of the total $M-N_{py}$ bond length displacement and are the only ones that vary between the three solutions. On the other hand, modes 7 and 8 together contribute less than 10% for the total displacements for any of the remaining bond length coordinates, so the ambiguity in the assigned phases for these modes is irrelevant to the remaining δr values compared to experimental uncertainty. The differences in the values of several of the bond angles calculated by the three solutions are more sensitive to the uncertainty in the three solutions since mode 7 contributes significantly to all of these coordinates. Consequently, no reasonable estimates can be made for the angular displacements.

The excited-state geometry displacements calculated for the three different metal complexes are slightly different. However, these differences are not sufficiently large that any statement can be made regarding the actual metal-related changes in the relative ground- and excited-state geometries. The geometry displacements obtained for the Fe(II) complex differ substantially from those obtained by Spiro and co-workers.[15] This is probably due to the fact that the Δ_s values are too large to assume the "small-displacement limit" as was done in their study.

V. Summary

1. The RR spectra of $(OEP)M(py)_2$, where M = Fe(II), Ru(II), or Os(II), are quite sensitive to the nature of the metal center. Frequency trends observed for the porphyrin skeletal modes are due to a complex interplay of effects, including alterations in metal–porphyrin bonding (both σ and π), changes in porphyrin core size, and variation of metal charge. No single effect is sufficient to account for all of the observed trends.

2. The vibronic activity of the porphyrin modes as evidenced in Q-state RRES exhibits noticeable trends with metal variation. The trends in vibronic activity can be mostly explained in terms of CI variation between the Q and B states of the porphyrin in a fashion consistent with that indicated by observed changes in the relative intensities of the Q(0,0) and B(0,0) absorption bands. Strong coupling between porphyrin modes is evidenced in Q-state RRES obtained for the Fe(II) complex but is not observed for either of the other two. This is consistent with decreased CI in the Ru(II) and Os(II) complexes, since vibronic coupling becomes less important to Q-state RR intensity as the Q-state absorption approaches that of the B state.

3. Metal(d_π) → py(π^*) CT states are located in the visible region of the absorption spectra of the $(OEP)M(py)_2$ series as evidenced by resonance enhancement of py vibrations in the RR spectra. CT states are located for all three complexes in the 500-nm region. A second CT state is located near 600 nm for the Os(II) complex and is due to the extremely large spin–orbit coupling of this metal.

4. The observed frequencies of the resonance-enhanced py modes of the three complexes are different than those of free py and show noticeable trends as functions of metal center. Normal mode analyses of metal-bound py indicate that kinetic energy and σ-bonding effects account for the observed trends and that the py force field (and therefore py π-electron distribution) is essentially independent of the metal. Excited-state origin shifts determined for the CT states of the three complexes also indicate that changes in the ground-state py π-electron distribution induced by varying the metal are quite small.

Table VII. Non-Zero Vibronic Terms Coupling the Components of the $Q^{0'}$ and $B^{0'}$ States[a]

	$Q_x^{0'}$	$Q_y^{0'}$	$B_x^{0'}$	$B_y^{0'}$
$Q_x^{0'}$	$(a_{1g}' + b_{1g}')\cos^2\theta + (a_{1g}'' + b_{1g}'')\sin\theta -$ $(a_{1g} + b_{1g})\sin 2\theta$	$(b_{2g}')\cos^2\theta + (b_{2g}'')\sin^2\theta -$ $(b_{2g})\sin 2\theta$	$\frac{1}{2}(a_{1g}' + b_{1g}' - a_{1g}'' - b_{1g}'')\sin 2\theta +$ $(a_{1g} + b_{1g})\cos 2\theta$	$\frac{1}{2}(b_{2g}' - b_{2g}'')\sin 2\theta + (b_{2g})\cos 2\theta \cdot a_{2g}$
$Q_y^{0'}$		$(a_{1g} - b_{1g}')\cos^2\theta + (a_{1g}'' - b_{1g}'')\sin^2\theta \cdot$ $(a_{1g} - b_{1g})\sin 2\theta$	$\frac{1}{2}(b_{2g}' - b_{2g}'')\sin 2\theta + (b_{2g})\cos 2\theta + a_{2g}$	$\frac{1}{2}(a_{1g}' + b_{1g}' - a_{1g}'' - b_{1g}'')\sin 2\theta +$ $(a_{1g} - b_{1g})\cos 2\theta$
$B_x^{0'}$			$(a_{1g}' + b_{1g}')\sin^2\theta + (a_{1g}'' + b_{1g}'')\cos^2\theta +$ $(a_{1g} + b_{1g})\sin 2\theta$	$(b_{2g}')\sin^2\theta + (b_{2g}'')\cos^2\theta + (b_{2g})\sin 2\theta$
$B_y^{0'}$				$(a_{1g}' - b_{1g}')\sin^2\theta + (a_{1g}'' - b_{1g}'')\cos^2\theta +$ $(a_{1g} - b_{1g})\sin 2\theta$

[a] $Q^{0'}$ and $B^{0'}$ refer to the Q and B states of the porphyrin for which the four-orbital model has been relaxed. In the four-orbital model, $a_{1g}' = a_{1g}'' \neq 0$ and $b_{1g}' = b_{1g}'' = b_{2g}' = b_{2g}'' = 0$ (see text). The Table is symmetric.

Acknowledgment is made to the donors of the Petroleum Research Fund, administered by the American Chemical Society, the Cottrell Research Grants Program of the Research Corporation, the Committee on Research, University of California, Riverside, and the National Institute of General Medical Sciences (GM-30078-01A1) for support of this research. Partial funding for the Raman spectrometer was provided by the Biomedical Research Support Grant Program of the U.S. Public Health Service. The authors thank Prof. W. R. Scheidt for communicating his results prior to publication and Prof. M. Gouterman, Prof. J. W. Buchler, and Dr. J. A. Shelnutt for helpful discussions.

Appendix

A. Metalloporphyrin-Mode RRES. The procedures used to simulate the RRES of porphyrin skeletal modes are based on the methods of Shelnutt.[20,49,53] We give a brief description of the model here since our expressions used to calculate intensity dispersions as functions of excitation frequency, though based on previous theory, have not been explicitly given elsewhere.

In the four-orbital model, the zero-order electronic basis set used to describe the properties of the porphyrin macrocycle consists of 50/50 mixtures of the two sets of doubly degenerate excited configurations, $(a_{1u})^1(a_{2u})^2(e_g)^1$ and $(a_{1u})^2(a_{2u})^1(e_g)^1$:[45]

$$\left.\begin{matrix}|B_x^0\rangle \\ |Q_x^0\rangle\end{matrix}\right\} = 2^{-1/2}[a_{2u}e_{yg} \mp a_{1u}e_{xg}] \qquad \text{(A-1a)}$$

$$\left.\begin{matrix}|B_y^0\rangle \\ |Q_y^0\rangle\end{matrix}\right\} = 2^{-1/2}[a_{2u}e_{xg} \pm a_{1u}e_{yg}] \qquad \text{(A-1b)}$$

A CI parameter, θ, is introduced as a measure of the "unmixing" of the configurations in eq A-1[49,53]

$$|Q_x\rangle = \cos\theta|Q_x^0\rangle - \sin\theta|B_x^0\rangle \qquad \text{(A-2a)}$$

$$|Q_y\rangle = \cos\theta|Q_y^0\rangle - \sin\theta|B_y^0\rangle \qquad \text{(A-2b)}$$

$$|B_x\rangle = \cos\theta|B_x^0\rangle + \sin\theta|Q_x^0\rangle \qquad \text{(A-2c)}$$

$$|B_y\rangle = \cos\theta|B_y^0\rangle + \sin\theta|Q_y^0\rangle \qquad \text{(A-2d)}$$

The transition dipoles also depend on θ. The μth components of the zero-order dipoles are defined by

$$r_\mu^0 = \langle G|e\tilde{\mu}|Q_\mu^0\rangle \qquad \text{(A-3a)}$$

$$R_\mu^0 = \langle G|e\tilde{\mu}|B_\mu^0\rangle \qquad \text{(A-3b)}$$

and the CI-unmixed transition dipoles are

$$r_\mu = r_\mu^0 \cos\theta - R_\mu^0 \sin\theta \qquad \text{(A-4a)}$$

$$R_\mu = r_\mu^0 \sin\theta + R_\mu^0 \cos\theta \qquad \text{(A-4b)}$$

The transition dipole, r_μ^0, is generally assumed to be zero.[44] Within the rigorous four-orbital model, JT activity is introduced only through the CI parameter θ since one-electron terms between the degenerate components of $|Q^0\rangle$ and $|B^0\rangle$ vanish.[63] Intrinsic JT activity can be introduced if the four-orbital model is relaxed; that is, the zero-order states contain excited-state configurations in addition to those given in eq A-1. In this case the porphyrin $\pi\pi^*$ excited states can be treated as two arbitrary states of E_u symmetry ($Q^{0\prime}$ and $B^{0\prime}$). The vibronic interactions in the arbitrary basis are shown in Table VII. It must be stressed that all of our calculations are performed in the arbitrary basis set. In this basis, the 50/50 mixed configurations of the four-orbital model have no real meaning and the parameter θ actually describes the degree of mixing of the arbitrary zero-order states ($Q^{0\prime}$ and $B^{0\prime}$).

The Raman intensity is proportional to the square modulus of the scattering tensor, $|\alpha|^2$, for the Q and B states and is given by

$$I \propto |\alpha(\nu_L)|^2 = \left|\frac{T_1}{E_{Q0} - \nu_L - i\Gamma_Q} + \frac{T_2}{E_{B0} - \nu_L - i\Gamma_B} + \frac{T_3}{E_{Q1_k} - \nu_L - i\Gamma_Q} + \frac{T_4}{E_{B1_k} - \nu_L - i\Gamma_B}\right|^2 \qquad \text{(A-5)}$$

where ν_L is the excitation frequency, Γ_Q and Γ_B are the line widths (HWHM) of the Q and B states, E_{Q0} and E_{B0} are the transition energies of the Q- and B-state origins, E_{Q1_k} and E_{B1_k} are the transition energies of the first vibronic states of the Q and B manifolds for the kth vibrational mode, and T_1 through T_4 are terms containing the electronic and vibronic integrals that depend on the nature of the kth mode. These latter terms for the B_g modes, which are considered in our calculations, are given by

$$T_1^{B_g} = -r_\mu'^2\left[\frac{b_g' \cos^2\theta + b_g'' \sin^2\theta - b_g \sin 2\theta}{\nu_k}\right] - r_\mu' R_\mu'\left[\frac{b_g \cos 2\theta + \frac{1}{2}(b_g' - b_g'')\sin 2\theta}{\Delta_{QB} + \nu_k}\right] \qquad \text{(A-6a)}$$

$$T_2^{B_g} = -R_\mu'^2\left[\frac{b_g' \sin^2\theta + b_g'' \cos^2\theta + b_g \sin 2\theta}{\nu_k}\right] + r_\mu' R_\mu'\left[\frac{b_g \cos 2\theta + \frac{1}{2}(b_g' - b_g'')\sin 2\theta}{\Delta_{QB} - \nu_k}\right] \qquad \text{(A-6b)}$$

$$T_3^{B_g} = r_\mu'^2\left[\frac{b_g' \cos^2\theta + b_g'' \sin^2\theta - b_g \sin 2\theta}{\nu_k}\right] - r_\mu' R_\mu'\left[\frac{b_g \cos 2\theta + \frac{1}{2}(b_g' - b_g'')\sin 2\theta}{\Delta_{QB} - \nu_k}\right] \qquad \text{(A-6c)}$$

$$T_4^{B_g} = R_\mu'^2\left[\frac{b_g' \sin^2\theta + b_g'' \cos^2\theta + b_g \sin 2\theta}{\nu_k}\right] + r_\mu' R_\mu'\left[\frac{b_g \cos 2\theta + \frac{1}{2}(b_g' - b_g'')\sin 2\theta}{\Delta_{QB} + \nu_k}\right] \qquad \text{(A-6d)}$$

In the calculations, the transition dipole, $r_\mu^{0\prime}$, has been taken to be zero.

B. Pyridine-Mode RRES. The RR intensities of totally symmetric modes primarily depend on the dipole strength of the electronic transition and on the FC overlaps of the ground- and excited-state vibrational wave functions. The RR intensity is proportional to the square of the polarizability dispersion which, in the harmonic approximation and assuming equal vibrational frequencies for the ground and excited states, is related to the FC products and the electronic dipole transition integral $M_{0\text{-}0}$, and is given for mode 1 by[62]

$$\alpha_{1\text{-}0} = M_{0\text{-}0}^2 \sum_{v_1}\sum_{v_2}\cdots\sum_{v_{3N-6}} \frac{\langle I_1|v_1\rangle\langle v_1|0_1\rangle \prod_{i=2}^{3N-6}|\langle v_i|0_i\rangle|^2}{\Delta\nu + \sum_{i=1}^{3N-6} v_i\nu_i + i\Gamma} \qquad \text{(B-1)}$$

Here the line widths, Γ, of the 0–0 and 0–1 electronic transitions have been assumed to be the same, ν_i is the vibrational frequency for mode i, and $\Delta\nu$ is the difference in frequency between the electronic transition origin and the excitation energy. The effects of inhomogeneous broadening are included by convoluting eq B-1 with a line shape function $g(\nu_i - \bar{\nu}_i)$, where $\bar{\nu}_i$ is the average energy

(63) Perrin, M. H.; Gouterman, M.; Perrin, C. L. *J. Chem. Phys.* **1969**, *50*, 4137–4150.

for a given mode. In our calculations $g(v_i - \bar{v}_i)$ was assumed to be a Gaussian function of width γ (HWHM) for every mode. The excited-state displacements are related to the FC factors through the relationships[64]

$$\langle v_i|0_i\rangle^2 = \frac{\Delta_i^{2v}}{2^v v!} e^{-\Delta_i^2/2} \quad \text{(B-2a)}$$

$$\langle 1_i|v_i\rangle\langle v_i|0_i\rangle = \frac{\Delta_i^{2v+1} - 2v\Delta_i^{2v-1}}{2^v 2^{1/2} v!} e^{-\Delta_i^2/2} \quad \text{(B-2b)}$$

(64) Inagaki, F.; Tasumi, M.; Miyazawa, T. *J. Mol. Spectrosc.* **1974**, *50*, 286-303.

where Δ_s is the shift in the excited state relative to the ground state along the normal coordinate s. The Cartesian displacements, δr, of the atoms for the excited state can be extracted from the origin shifts via the transformation[15,61]

$$\delta r_i = (m_i)^{-1/2} \sum_s L_{si}\Delta_s / 0.17 \nu_s^{1/2} \quad \text{(B-3)}$$

where L_{si} is the eigenvector element that connects atom i having mass m_i with the normal mode s (this assumes that the normal modes have the same form in the ground and excited states).

Registry No. [(OEP)Fe(py)$_2$], 19496-63-0; [(OEP)Ru(py)$_2$], 54762-60-6; [(OEP)Os(py)$_2$], 51286-87-4; deuterium, 7782-39-0.

Positive Halogen Cryptates[1]

Raymond Le Goaller, Henri Handel, Pierre Labbe, and Jean-Louis Pierre*

Contribution from the Laboratoire d'Etudes Dynamiques et Structurales de la Sélectivité II, Université Scientifique et Médicale de Grenoble, BP 68, 38041 Saint Martin D'Heres Cedex, France. *Received December 27, 1982*

Abstract: Interactions of molecular bromine or iodine with [2.2.2], [2.2.1], and [2.1.1] cryptands were examined in chloroform. NMR measurements evidence a 1:1 complex in each case and allow the determination of the kinetic parameters for the decomplexation process. UV spectroscopy permits the determination of the equilibria constants. The complexes are destroyed (displacement of "X^+") by addition of either a protic acid or an alkaline metal salt. The results taken as a whole strongly suggest the conclusion that the complexes are positive halogen cryptates.

The formation of charge-transfer complexes between diatomic halogens and amines or ethers has been extensively investigated.[2] In these complexes a linear orientation of the halogen molecule with the donor atom is observed in the solid state. In solution, in the case of amines, the occurrence of ionic species has been considered.

Cationic species X_2^+ and X_3^+ were shown to be present in superacid media, but no direct evidence has been found for the occurrence of the cations X^+ either in solution or in the solid state,[3] although their intervention in the course of electrophilic halogenation reactions seems to be accepted.

Macrocyclic polyethers exhibit remarkable complexing properties toward metallic ions whose size fits their cavity's diameter.[4] It seemed interesting to us to investigate the potential complexing ability of these macrocycles toward positive halogen ions formed by induced dissociation of halogen molecules.[5]

Crown ethers do not seem to effect this transformation. Indeed Short[6] and Pannell[7] have shown that bromine forms the same type of charge-transfer complexes with crown ethers and single ethers. Although the presence of ionic species had been postulated, Hopkins[8] obtained, for the complexes of iodine with crown ethers, stability constants of the same order of magnitude as those obtained with simple ethers. Table I summarizes some results reported in the literature.

Table I. 1:1 Complexes

complex	solvent	K_s, L M^{-1} at 25 °C	ref
1,4-dioxane-Br_2	CCl_4-EtBr (3:1)	1.2	7
18-6-crown-Br_2	CCl_4-EtBr (3:1)	1.0	7
THF-I_2	cyclohexane	2.54	8
18-6-crown-I_2	cyclohexane	4.93	8
Et_3N-I_2	heptane	4690	2
18-6-crown-K^+	MeOH	$10^{6.1}$	4
[2.2.2] cryptand-K^+	MeOH (95%)	$10^{9.75}$	4

Table II. 100-MHz NMR Spectra of 10^{-1} M Solutions in $CDCl_3$ at −15 °C for the [2.2.2] Cryptand-I_2 1:1 Complex (δ in ppm)

complex	$-OCH_2CH_2O-$ (s)	$-OCH_2CH_2N$ (t)	$-CH_2N$ (t)
[2.2.2]	3.69	3.60	2.65
[2.2.2]-I_2	3.65	3.70	3.23
[2.2.2]-Br_2	3.65	3.80	3.30
[2.2.1]	3.69	3.60	2.68
[2.2.1]-I_2	3.71	3.65	3.25
[2.2.1]-Br_2	3.70	~3.70	3.35
[2.1.1]	3.66	3.51	2.71
[2.1.1]-I_2	3.65	3.73	3.35
[2.1.1]-Br_2	3.65	3.70	3.35

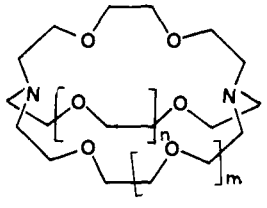

Figure 1. Cavity diameters of cryptands: [2.2.2], $m = n = 1$, 2.8 Å; [2.2.1], $m = 1$ and $n = 0$, 2.3 Å; [2.1.1], $m = n = 0$, 1.6 Å.

Results

In order to investigate the possible effects of cavity size[5] (Figure 1) three different cryptands were used in this study, namely [2.2.2], [2.2.1], and [2.1.1]. The halogens used were molecular iodine

(1) Preliminary communication: Pierre, J. L.; Handel, H.; Labbe, P.; Le Goaller, R. *J. Am. Chem. Soc.* **1980**, *102*, 6574.
(2) Foster, R. "Organic Charge-Transfer Complexes"; Academic Press: New York, 1969.
(3) Effenberger, F. *Angew. Chem., Int. Ed. Engl.* **1980**, *19*, 151.
(4) "Synthetic Multidentate Macrocyclic Compounds"; Izatt, R. M., Christensen, J. J., Eds.; Academic Press: New York, 1979.
(5) The evaluation of ionic radius by the Sanderson method allows one to consider the cryptation of X^+ species: rI^+ 0.6-0.8 Å; rBr^+ 0.45-0.72 Å (the first value corresponds to the cation in a gaseous phase; the second to the coordinated cation).
(6) Schori, E.; Jagur-Grodzenski, J. *Israel J. Chem.* **1972**, *10*, 935.
(7) Pannell, K. H.; Mayr, A. *J. Chem. Soc., Chem. Commun.* **1979**, 132.
(8) Hopkins, H. P.; Jahagirdar, D. V.; Winder, F. J. *J. Phys. Chem.* **1978**, *82*, 1254.

0002-7863/84/1506-1694$01.50/0